Separation and Characterization of Currents through Store-operated CRAC Channels and Mg^{2+}-inhibited Cation (MIC) Channels

Murali Prakriya and Richard S. Lewis

Department of Molecular and Cellular Physiology, Stanford University School of Medicine, Stanford, CA 94305

ABSTRACT Although store-operated calcium release–activated Ca^{2+} (CRAC) channels are highly Ca^{2+}-selective under physiological ionic conditions, removal of extracellular divalent cations makes them freely permeable to monovalent cations. Several past studies have concluded that under these conditions CRAC channels conduct Na^+ and Cs^+ with a unitary conductance of ~40 pS, and that intracellular Mg^{2+} modulates their activity and selectivity. These results have important implications for understanding ion permeation through CRAC channels and for screening potential CRAC channel genes. We find that the observed 40-pS channels are not CRAC channels, but are instead Mg^{2+}-inhibited cation (MIC) channels that open as Mg^{2+} is washed out of the cytosol. MIC channels differ from CRAC channels in several critical respects. Store depletion does not activate MIC channels, nor does store refilling deactivate them. Unlike CRAC channels, MIC channels are not blocked by SKF 96365, are not potentiated by low doses of 2-APB, and are less sensitive to block by high doses of the drug. By applying 8–10 mM intracellular Mg^{2+} to inhibit MIC channels, we examined monovalent permeation through CRAC channels in isolation. A rapid switch from 20 mM Ca^{2+} to divalent-free extracellular solution evokes Na^+ current through open CRAC channels (Na^+-I_{CRAC}) that is initially eightfold larger than the preceding Ca^{2+} current and declines by ~80% over 20 s. Unlike MIC channels, CRAC channels are largely impermeable to Cs^+ (P_{Cs}/P_{Na} = 0.13 vs. 1.2 for MIC). Neither the decline in Na^+-I_{CRAC} nor its low Cs^+ permeability are affected by intracellular Mg^{2+} (90 μM to 10 mM). Single openings of monovalent CRAC channels were not detectable in whole-cell recordings, but a unitary conductance of 0.2 pS was estimated from noise analysis. This new information about the selectivity, conductance, and regulation of CRAC channels forces a revision of the biophysical fingerprint of CRAC channels, and reveals intriguing similarities and differences in permeation mechanisms of voltage-gated and store-operated Ca^{2+} channels.

KEY WORDS: calcium channel • calcium signaling • ion/membrane channel • TRP-PLIK • LTRPC7

INTRODUCTION

The depletion of Ca^{2+} from the ER in nonexcitable cells triggers Ca^{2+} influx across the plasma membrane, a process termed store-operated Ca^{2+} entry. Store-operated channels (SOCs)* are widely, if not ubiquitously, expressed in nonexcitable cells, where they provide a major route for Ca^{2+} entry (for reviews see Parekh and Penner, 1997; Lewis, 1999; Putney and McKay, 1999). One of the best described SOCs, the calcium release–activated Ca^{2+} (CRAC) channel, is present in mast cells, T lymphocytes, and several related cell lines. CRAC channels influence a variety of important physiological processes, including the release of inflammatory mediators from mast cells during allergic reactions, and the generation of $[Ca^{2+}]_i$ oscillations leading to gene expression and the differentiation and activation of T cells (for reviews see Parekh and Penner, 1997; Lewis, 2001). The critical role of CRAC channels in human physiology is shown clearly by the devastating immunodeficiencies that arise from the absence of CRAC channel activity in T cells from human patients (Partiseti et al., 1994; Feske et al., 2001).

In view of their critical physiological functions, considerable effort has been focused on isolating the gene(s) encoding the CRAC channel and on understanding how the channel's gating is regulated. Although several genes of the TRP family have been proposed to encode the CRAC channel, it is unclear as to whether the currents resulting from heterologous expression of these genes are identical to native I_{CRAC} (Putney and McKay, 1999; Clapham et al., 2001; Prakriya and Lewis, 2002). Several classes of activation mechanisms are currently being studied, including a diffusible messenger released from the ER, depletion-triggered insertion of CRAC channels into the plasma membrane, and physical coupling between the channels and IP_3 receptors in the ER. However, there is as yet no consensus on which if any of these mechanisms may be correct (Putney et al., 2001). Progress in resolving these issues has been hampered by several factors that are unique to this class of channels, including a lack of selective inhibitors, very small whole cell cur-

Address correspondence to Richard S. Lewis, Beckman Center B-111A, Stanford University School of Medicine, Stanford, CA 94305. Fax: (650) 725-8021; E-mail: rslewis@stanford.edu

*Abbreviations used in this paper: 2-APB, 2-aminoethyldiphenyl borate; CDP, Ca^{2+}-dependent potentiation; CRAC, calcium release–activated Ca^{2+}; DVF, divalent-free; MIC, Mg^{2+}-inhibited cation; SOC, store-operated channel; TG, thapsigargin.

rents (on the order of a few pA per cell), and an extremely small single-channel Ca^{2+} conductance (2–26 fS estimated from noise analysis) (Zweifach and Lewis, 1993), which has precluded single-channel recording in membrane patches.

The study of currents carried by monovalent cations through CRAC channels could, in principle, bypass some of these problems. Like voltage-gated Ca^{2+} channels (Almers and McCleskey, 1984; Hess et al., 1986), CRAC channels under physiological conditions are exquisitely selective for Ca^{2+}, conducting Ca^{2+} ~1,000 times better than the more prevalent Na^+ (Hoth and Penner, 1993; Hoth, 1995). However, as with voltage-gated Ca^{2+} channels (Almers and McCleskey, 1984), the removal of extracellular divalent cations renders CRAC channels permeable to Na^+ (Hoth and Penner, 1993; Lepple-Wienhues and Cahalan, 1996). Initially, upon removal of extracellular divalents, this Na^+ current is approximately six times larger than the preceding Ca^{2+} current, but it declines by >90% over tens of seconds. The slow loss of channel activity is reversed following readdition of extracellular Ca^{2+}, a process referred to as Ca^{2+}-dependent potentiation (CDP) (Christian et al., 1996b; Zweifach and Lewis, 1996). Kerschbaum and Cahalan (1998) found that removal of intracellular Mg^{2+} made the Na^+ current larger and sustained, leading to the idea that intracellular Mg^{2+} is required for CRAC channel depotentiation. Furthermore, in the absence of intracellular Mg^{2+} the whole-cell current was seen to arise from the progressive, all-or-none activation of single 40-pS channels having a high open probability ($P_o > 0.9$) (Kerschbaum and Cahalan, 1999). Similar results were later found in human T cells (Fomina et al., 2000) and RBL cells (Braun et al., 2001). The Na^+ currents were considered to arise from CRAC channels based on their slow time course of activation and inhibition by extracellular Ca^{2+}, Mg^{2+}, Ni^{2+}, and Gd^{3+} (Kerschbaum and Cahalan, 1999; Fomina et al., 2000; Braun et al., 2001). These results are significant because resolution of CRAC currents at the single-channel level is expected to greatly facilitate studies of the molecular mechanism of store-operated Ca^{2+} entry. In fact, the conductance, selectivity, and high open probability of the Na^+-conducting channels was exploited in studies of the CRAC channel's activation mechanism (Braun et al., 2001; Rychkov et al., 2001), changes in CRAC channel expression during T cell activation (Fomina et al., 2000), and for the identification of genes that may encode the CRAC channel pore region (Yue et al., 2001).

Although the discovery of the large, sustained monovalent current in the absence of intracellular Mg^{2+} has offered new opportunities for molecular characterization of CRAC channels, we noted several discrepancies in our own studies which led us to examine its identity in greater detail. We have found that the large sustained monovalent current seen with Mg^{2+}-free intracellular solutions arises from a store-independent channel that differs from I_{CRAC} in its ion selectivity, pharmacology, and regulation. Because its activity is suppressed by intracellular Mg^{2+}, we refer to this channel as the Mg^{2+}-inhibited cation (MIC) channel. By using conditions that prevent the activation of I_{MIC}, we have been able to characterize monovalent fluxes through CRAC channels. Several key properties of monovalent CRAC channels, including ion selectivity, unitary conductance, and regulation by intracellular Mg^{2+}, differ significantly from those described previously. These new results reveal similarities and differences in the ionic selectivity mechanisms of store-operated and voltage-gated Ca^{2+} channels, and force a revision of the biophysical fingerprint of CRAC channels that will have important implications for the identification of CRAC channel genes.

MATERIALS AND METHODS

Cells

Jurkat E6-1 human leukemic T cells (American Type Culture Collection) were grown in a medium consisting of RPMI 1640 supplemented with 10% fetal calf serum, 2 mM glutamine, 50 U/ml penicillin and 50 μg/ml streptomycin. The cells were maintained in log-phase growth at 37°C in 6% CO_2.

Solutions and Chemicals

The standard extracellular Ringer's solution contained (in mM): 155 NaCl, 4.5 KCl, 2 or 20 $CaCl_2$, 1 $MgCl_2$, 10 D-glucose, and 5 Na-HEPES (pH 7.4). Ca^{2+}-free Ringer's was prepared by substituting 1 mM EGTA + 2 mM $MgCl_2$ for $CaCl_2$. The divalent-free (DVF) Ringer's solutions contained (in mM): 155 Na, Cs, or NMDG methanesulfonate, and 10 HEDTA, 1 EDTA and 10 Hepes (pH 7.4 with NaOH, CsOH, or HCl, respectively). The standard internal solution contained (in mM): 150 Cs methanesulfonate, 3–10 mM $MgCl_2$, 10 BAPTA, and 10 Cs-Hepes (pH 7.2). The Mg^{2+}-free (MGF) intracellular solution contained (in mM): 150 Cs methanesulfonate, 10 HEDTA, 0.5 $CaCl_2$ (calculated $[Ca^{2+}]_i$ = 10 nM) and 10 Cs-Hepes (pH 7.2). Where noted, 10 mM BAPTA was substituted for HEDTA. In the experiments on I_{CRAC} deactivation, the intracellular solution contained (in mM): 150 Cs methanesulfonate, 2 mM CsCl, 1.2 EGTA or 1 BAPTA, and 10 Cs-HEPES (pH 7.2). In the excised patch experiments, the pipette solution contained an Na-based DVF solution (composition listed above), and the cytoplasmic face of the patch was exposed to the MGF solution (listed above, but with 0 $CaCl_2$) to which an appropriate quantity of $MgCl_2$ added to yield the free $[Mg^{2+}]$ indicated in the figure legends. MgATP and Na_2ATP (Sigma-Aldrich) were added to the intracellular solution in some experiments, and free $[Mg^{2+}]_i$ and $[Ca^{2+}]_i$ were calculated using MaxChelator software (WEBMAXC 2.10, available at http://www.stanford.edu/~cpatton/webmaxc2.htm).

2-aminoethyldiphenyl borate (2-APB) was provided by Dr. K. Mikoshiba (Tokyo University, Japan). In some experiments, 2-APB obtained from Sigma-Aldrich was used; no difference was found between the drugs from the different sources. Stock solutions of 2-APB and thapsigargin (Sigma-Aldrich) were prepared in DMSO at concentrations of 20 mM and 1 mM, respectively; SKF 96365 (Sigma-Aldrich) was dissolved in deionized water at a concentration of 10 mM. The drugs were diluted to the concen-

trations indicated in the legends and applied to the cells using a multi-barrel local perfusion pipette with a common delivery port. The time for 90% solution exchange was measured to be <1 s, based on the rate at which the K^+ current reversal potential changed when the external $[K^+]$ was switched from 2 to 150 mM.

Patch-Clamp Measurements

Patch-clamp experiments were conducted in the standard whole-cell recording configuration at 22–25°C using an Axopatch 200 amplifier (Axon Instruments, Inc.), an ITC-16 interface (Instrutech) and a Macintosh G3 computer. Recording electrodes were pulled from 100-μl pipettes coated with Sylgard and fire-polished to a final resistance of 2–5 MΩ. Stimulation and data acquisition and analysis were performed using in-house routines developed on the Igor Pro platform (Wavemetrics). The holding potential was 20 mV unless otherwise indicated. Voltage stimuli usually consisted of a 100-ms step to −110 mV, immediately followed by a 100-ms ramp from −110 to 90 mV applied every 1–2 s. Currents were filtered at 1 kHz with a 4-pole Bessel filter and sampled at 5 kHz without series resistance compensation. Data are corrected for the liquid junction potential of the pipette solution relative to Ringer's in the bath (−10 mV) and of the bath DVF solution relative to Ringer's in the bath-ground agar bridge (5 mV). The averaged results are presented as the mean value ± SEM. Curve fitting was done by least-squares methods using built-in functions in Igor Pro 4.0. For the analysis of MIC channel kinetics, excised patches showing the activity of only one MIC channel were selected and processed using TAC (Bruxton Corporation). Channel transitions were idealized by setting a discriminator at 50% of the current between the open and closed levels, and the channel kinetics were obtained from the idealized traces.

Leak Current Subtraction

The activity of MIC channels when $[Mg^{2+}]_i$ is ≤3 mM (conditions of the majority of published papers on I_{CRAC}) can pose special problems for the isolation of I_{CRAC} in Jurkat cells. In our experience, MIC activity often changes significantly during the course of whole-cell recording (depending, among other things, on the free $[Mg^{2+}]$ in the pipette). Thus, the commonly employed practice of subtracting the current present at the start of whole-cell recording (before I_{CRAC} induction) from later currents will not necessarily isolate I_{CRAC} cleanly. A more consistent leak subtraction method is to expose the cell to a Ca^{2+}-free extracellular solution (0 Ca^{2+}/3 Mg^{2+}) shortly before or after measurement of the Ca^{2+} current, and to use this current as the "leak," because these ionic conditions eliminate I_{CRAC} (Zweifach and Lewis, 1993), but not I_{MIC} (see Fig. 7 C). Therefore, we used the zero-Ca^{2+} leak subtraction method to isolate I_{CRAC} in the experiments reported here. For measurements of I_{MIC}, leak current was collected in 20 mM Ca^{2+} immediately after whole-cell break-in.

Current Fluctuation Analysis

Current noise data were recorded using two methods. In the first, current at a holding potential of −110 mV was recorded continuously at 32-kHz bandwidth onto digital audio tape (Sony DTC-700 modified for DC coupling). For mean-variance analysis, data from tape were then lowpass-filtered at 2 kHz (8-pole Bessel filter; Frequency Devices) and digitized at 5 kHz for analysis. In the second method, current during 500-ms voltage steps to −110 mV applied once per second was lowpass-filtered at 1 kHz, digitized at 5 kHz, and recorded directly to hard disk. The series resistance was typically ∼5 MΩ, which in conjunction with the average membrane capacitance of 10 pF creates a 1-pole rolloff characteristic at 3.2 kHz; this filtering was ignored as it occurred well above the 1–2 kHz 8-pole Bessel cutoff we applied. The mean and variance were calculated from 200-ms segments of the digitized current. This short duration was chosen to minimize changes due to depotentiation of Na^+-I_{CRAC} during each sweep (<2% change in current). For spectral analysis, data from tape were replayed through a 20-Hz highpass filter (Krohn-Hite) and a 2-kHz lowpass Bessel filter (Frequency Devices) in series and were digitized at 5 kHz. Power spectra were computed from 512-point sweeps using a Hanning window (Igor Pro; Wavemetrics) and were averaged.

RESULTS

Induction of a Large Monovalent Conductance by Washout of Intracellular Mg^{2+}

As described in previous studies of Jurkat and human T cells (Kerschbaum and Cahalan, 1998, 1999; Fomina et al., 2000) and RBL cells (Braun et al., 2001), intracellular dialysis with Mg^{2+}-free internal solution in the absence of extracellular divalent cations triggers the slow development of a large monovalent conductance. In the experiment shown in Fig. 1, a Jurkat cell was dialysed with a Mg^{2+}-free intracellular solution containing HEDTA, and continuous exposure to a DVF Ringer's solution revealed the induction of a large inward current over a period of ∼400 s (Fig. 1 A). With equimolar extracellular Na^+ and intracellular Cs^+, the current reversed at −5 mV (Fig. 1 B), indicating approximately equal permeabilities for Na^+ and Cs^+. Substitution of NMDG for Na^+ selectively suppressed the inward current, demonstrating that the larger cation cannot permeate (Fig. 1, A and B). Early in the induction phase of the whole-cell current, the progressive opening of single channels could be resolved (Fig. 1 C). These channels generally opened in an all-or-none fashion to a very high open probability (P_o = 0.97 at −110 mV; n = 4 cells), such that openings of more than five channels could be clearly resolved under whole-cell conditions as described previously (Kerschbaum and Cahalan, 1999; Fomina et al., 2000). Based on the amplitude and reversal potential of the single-channel current, the average chord conductance was 44 ± 3 pS. We observed similar single-channel and whole-cell currents in human T cells freshly isolated from blood, although their activation following break-in was slower (unpublished data).

With DVF Ringer's in the recording pipette, these channels could also be observed in cell-attached patches and after patch excision into a Mg^{2+}-free intracellular solution (Fig. 1, D and E). These channels were similar to those seen in whole-cell recordings (Fig. 1 C) in terms of their conductance, lack of selectivity, high open probability, and brief closures. The channels were weakly voltage-dependent, with the average P_o changing from 0.97 at −135 mV to 0.84 at −55 mV (n = 4 patches). Kinetic analysis indicated that the mean closed time (τ_c) varied from 1.1 ± 0.1 ms at −135 mV to 7.9 ± 1.5 ms at −55 mV (n = 4 patches), whereas the

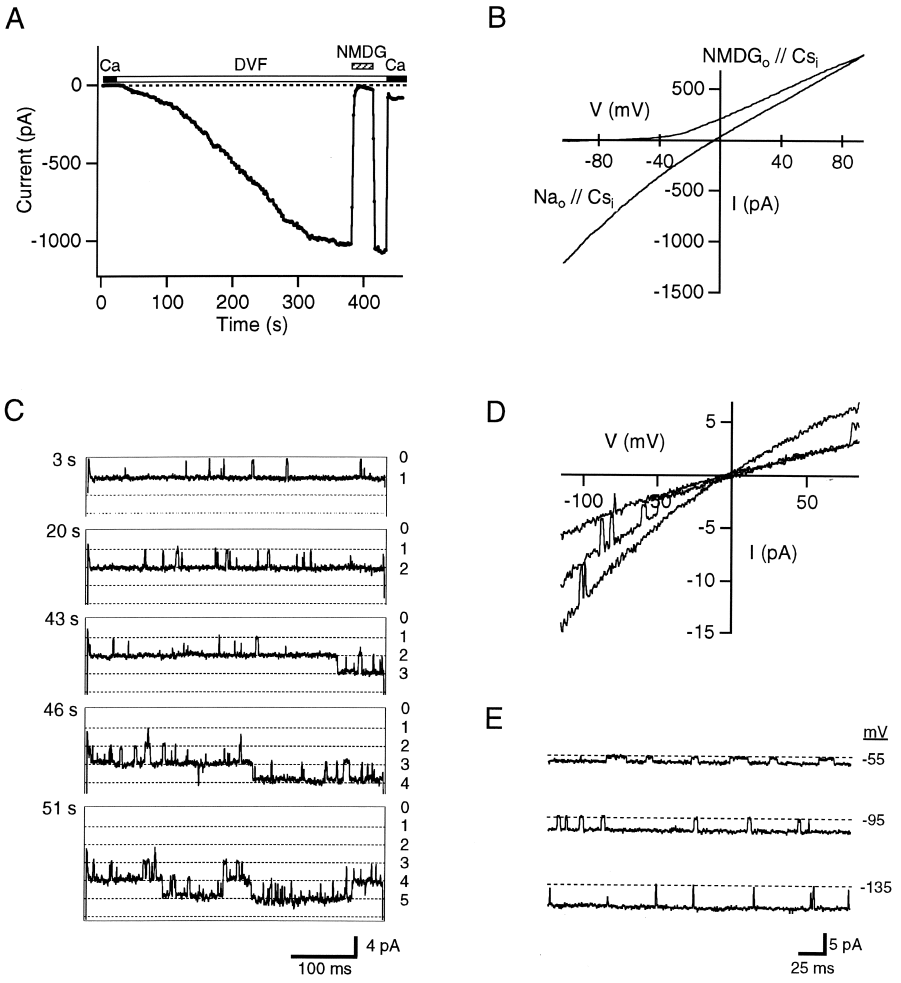

FIGURE 1. Activation of monovalent current in a Jurkat cell in the absence of extracellular divalent ions and intracellular Mg^{2+}. (A) Time course and selectivity of the current developing in the presence of DVF extracellular solution. The bar indicates sequential changes in the bath solution from 20 mM Ca^{2+} Ringer's to Na^+-DVF to NMDG-DVF (see MATERIALS AND METHODS). Each point represents the mean current during 100-ms steps to −110 mV, after subtraction of the leak current recorded in 20 mM Ca^{2+} immediately after break-in (time = 0). Internal solution: Cs methanesulfonate/10 HEDTA/0 Mg^{2+} (MGF). (B) Current-voltage relationship from the cell in A recorded with Na^+- or NMDG-based DVF extracellular solution. A 100-ms voltage ramp from −110 to 90 mV was applied. (C) Currents at −110 mV recorded at early times after break-in show progressive activation of single Na^+-conducting channels. Channels appear to activate sequentially, opening to very high probabilities in an all-or-none fashion. Numbers on the left indicate time after whole-cell break-in; numbers on the right indicate multiples of −3.9 pA. Same experimental protocol as in A, from another cell. (D) Current-voltage relationship of single channels conducting monovalent ions in an inside-out patch. Same voltage protocol as in B. Bath solution: MGF. Pipette solution: Na^+-DVF. (E) Single-channel currents at different potentials in an excised patch. Same conditions as in D. The closed level is indicated by the dashed lines.

mean open time was relatively constant (32.2 ± 3.5 ms at −135 mV and 36.3 ± 4.8 ms at −55 mV). In terms of unitary conductance, kinetics, open probability and reversal potential, these channels closely resemble the 40-pS channels described previously in Jurkat, human T cells, and RBL cells (Kerschbaum and Cahalan, 1998, 1999; Fomina et al., 2000; Braun et al., 2001).

In previous studies, the large, sustained monovalent current and the underlying 40-pS single-channel currents were ascribed to the activity of CRAC channels (Kerschbaum and Cahalan, 1998, 1999; Fomina et al., 2000; Braun et al., 2001). However, we noted several discrepancies in our own experiments that led us to question this conclusion. First, monovalent inward current under Mg^{2+}_i-free conditions activated much more slowly than the Ca^{2+} current in the presence of 20 mM extracellular Ca^{2+}, with half times of 210 ± 27 s (n = 5) and 109 ± 16 s (n = 6), respectively. Second, the ratio of I_{Ca} to I_{Na} varied widely among cells (from 13 in Fig. 1 A to more than 100), even to the point where monovalent currents in the nA range occurred in some cells lacking a measurable Ca^{2+} current. Finally, using a DVF pipette solution we observed 40-pS channels in the majority of cell-attached patches from resting cells in which stores were not deliberately depleted, suggesting that the large monovalent current may be store-independent. To determine whether it does in fact reflect CRAC channel activity, we compared its dependence on store depletion and its pharmacological profile with that of I_{CRAC}.

The Large Monovalent Current Does Not Activate and Deactivate in Parallel With I_{CRAC}

If the large monovalent current flows through CRAC channels, then it should be active immediately upon establishing the whole-cell recording configuration in cells with empty Ca^{2+} stores. To test this, 1 μM thapsigargin (TG) was applied for 5–10 min before seal formation to fully deplete stores and maximally activate CRAC channels. Soon after break-in to the whole-cell

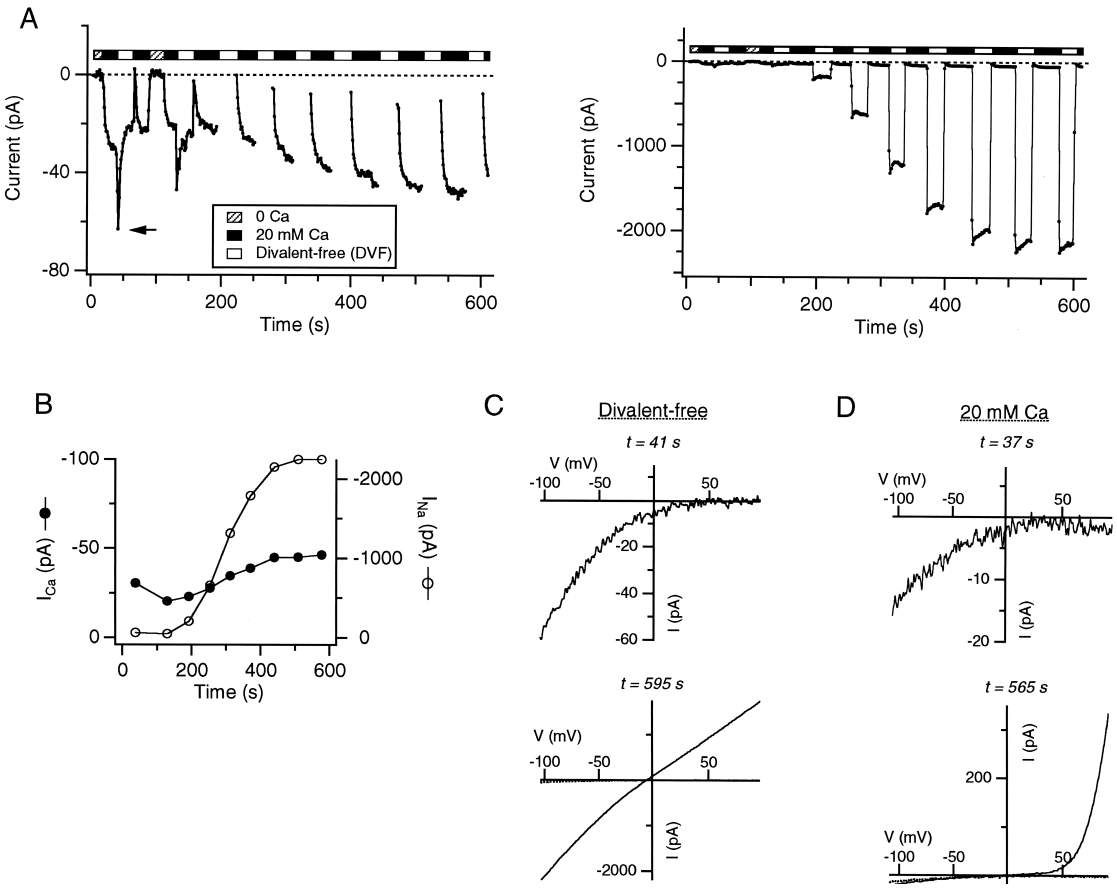

FIGURE 2. Depletion of Ca^{2+} stores does not activate the large monovalent current. (A) Activation of Ca^{2+} and Na^+ currents in a Jurkat cell treated with 1 μM TG for 5 min before seal formation. Current at −110 mV (corrected for leak current collected in 0 Ca^{2+} Ringer's) is plotted against time after break-in. As indicated by the bar, the extracellular solution was periodically switched between a 20 mM Ca^{2+} Ringer's and standard DVF solution to measure the Ca^{2+} and Na^+ currents, respectively. (left graph) The Ca^{2+} current I_{CRAC} is present at the time of break-in, and at these early times only a small transient Na^+ current is seen under DVF conditions (arrow). Large currents outside the graph boundaries are omitted for clarity. (Right graph) The same experiment at lower gain shows the slow development of a large Na^+ current in DVF solution following break-in. Internal solution: MGF. (B) Plot of the peak Ca^{2+} (●) and Na^+ (○) currents measured during applications of 20 mM Ca^{2+} or DVF solutions, respectively. (C) Monovalent current-voltage relationships recorded under DVF conditions early (41 s; small transient current in A) and late (595 s; large sustained current in A) in the experiment. Note the changes in size, rectification, and reversal potential of the current with time. (D) Current-voltage relations recorded in the presence of 20 mM Ca^{2+} at early (37 s) and late (565 s) times. A large outwardly rectifying current develops with time. In C and D, the currents from the upper graphs are reproduced as dashed lines in the lower graphs for comparison.

configuration, application of 20 mM Ca^{2+} to the cell causes an inward current to develop over ~10 s (Fig. 2 A). This inward current is I_{CRAC} as judged from its current-voltage relationship (Fig. 2 D, top graph), $Ca^{2+}{}_o$- and store-dependence, sensitivity to various pharmacological agents (unpublished data), and characteristic delayed appearance following each application of Ca^{2+}. This latter process, termed CDP, has been described previously (Zweifach and Lewis, 1996). Following Ca^{2+} readdition, the first application of DVF solution revealed only a small, transient inward Na^+ current at −110 mV that declined >60% within 20 s (arrow, Fig. 2 A). Subsequent short applications of DVF solution revealed the slow development of a large Na^+ current over the next 400 s, shown more clearly at lower gain (Fig. 2 A, right graph). Two observations suggest that the large Na^+ current and I_{CRAC} are not related. First, the amplitudes of the inward Ca^{2+} and Na^+ currents did not increase in parallel (Fig. 2 B), causing the ratio of the Na^+ to the Ca^{2+} current to change from ~2:1 at the beginning of the experiment (t = 37 s) to ~50:1 at later times (t = 570 s). Thus, the amplitudes of the Ca^{2+} current and the large Na^+ current are not well correlated in time. Second, during each application of DVF, the large Na^+ current was roughly constant, even though CRAC channels appeared to be closing. This is shown by the small initial Ca^{2+} current seen immediately after each Ca^{2+} readdition, followed by a prominent increase due to CDP. Similar results were obtained in five cells.

Importantly, several key properties of the monovalent currents changed during the experiment. Whereas the Na^+ current seen at early times in DVF solution decayed

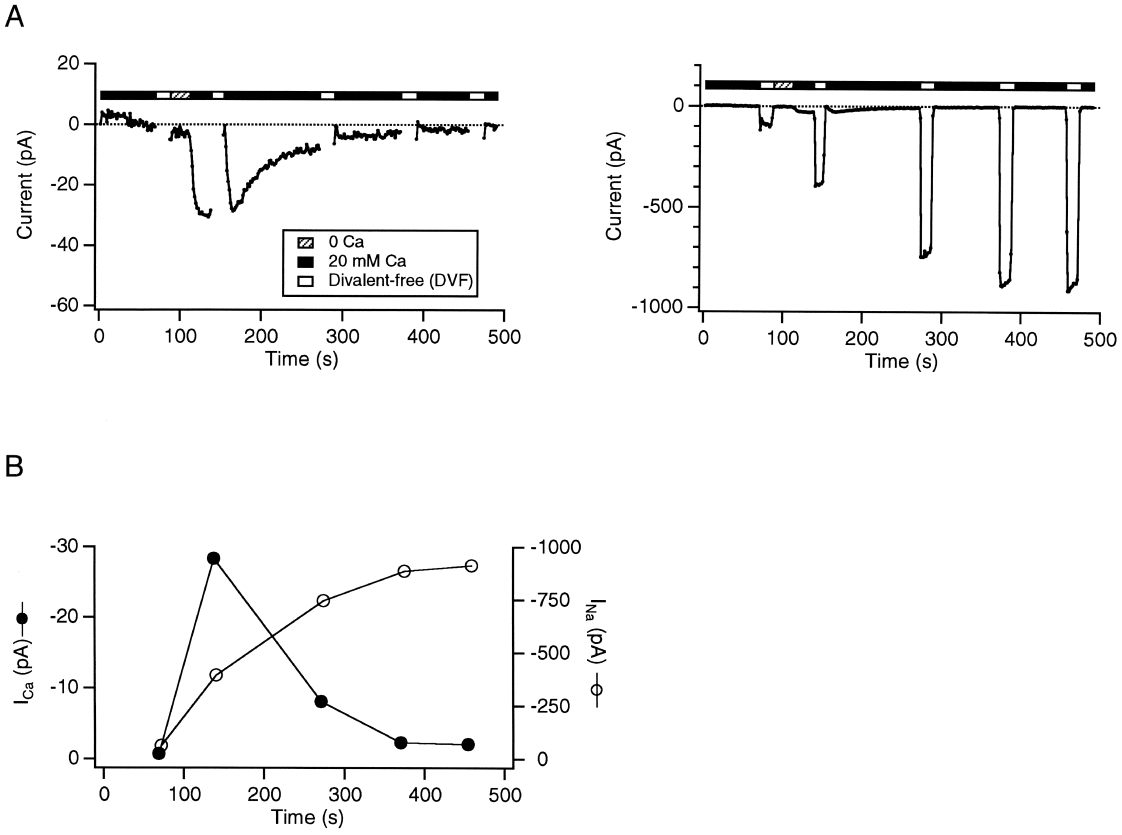

FIGURE 3. I_{CRAC} and the large monovalent current do not deactivate in parallel. (A) Following store depletion by passive dialysis with 1.2 mM EGTA, exposure to 20 mM Ca^{2+} evokes I_{CRAC}, which progressively declines due to elevation of intracellular $[Ca^{2+}]_i$ and refilling of Ca^{2+} stores. Current at −110 mV (corrected for leak current collected in 0 Ca^{2+} Ringer's) is plotted against time after break-in. Periodic exposure to DVF solution shows the development of the large monovalent current, shown at lower gain in the right graph. Note that I_{CRAC} depotentiates during the second exposure to DVF (left), even though the Na^+ current during that same period is fairly constant (right). Internal solution: Cs methanesulfonate/1.2 EGTA/0 Mg^{2+}. (B) The Ca^{2+} (●) and Na^+ currents (○) measured immediately before and during applications of the DVF solution in A. The monovalent current continues to increase as I_{CRAC} deactivates.

rapidly, at later times ($t > 200$ s) it was more sustained (Fig. 2, A and B). Second, the shape of the current-voltage relationship changed dramatically. At early times the monovalent current showed no clear reversal potential, even up to 90 mV, suggesting that intracellular Cs^+ permeates poorly if at all compared with Na^+ (Fig. 2 C, top), whereas at later times the current did not rectify and reversed near 0 mV, consistent with equal permeabilities for the two ions (Fig. 2 C, bottom). Time-dependent changes in current selectivity and rectification were also observed in the presence of extracellular Ca^{2+}. At the beginning of the experiment ($t < 50$ s), the whole-cell current in 20 mM $Ca^{2+}{}_o$ displayed prominent inward rectification, characteristic of I_{CRAC} (Fig. 2 D, top). However, at later time points (>300 s) the whole-cell current displayed strong outward rectification, generating a large outward current at potentials above 50 mV (Fig. 2 D, bottom). A likely explanation for these results is that an additional type of channel, unrelated to CRAC, activates slowly and produces a large, sustained and nonselective monovalent current that eventually dominates the whole-cell current under DVF conditions, and produces the outwardly rectifying current seen in the presence of Ca^{2+}. An alternative explanation (Kerschbaum and Cahalan, 1998) is that gradual removal of intracellular Mg^{2+} changes the properties of the CRAC channel, keeping it from inactivating and allowing it to conduct Cs^+ more efficiently.

To distinguish between these possibilities, we asked whether the large monovalent conductance deactivates in parallel with I_{CRAC} in response to store refilling. We have shown previously that in the presence of weak intracellular Ca^{2+} buffering (1 mM EGTA in the pipette solution), prolonged Ca^{2+} influx through CRAC channels can overwhelm the buffer, causing a global rise of $[Ca^{2+}]_i$, store refilling, and deactivation of I_{CRAC} (Zweifach and Lewis, 1995). This behavior is illustrated in the experiment of Fig. 3 A (left graph), in which I_{CRAC} measured in the presence of 20 mM Ca^{2+} activated slowly in response to passive store depletion, rose to a peak, then declined over ~150 s back to baseline. DVF solution was applied periodically in this experiment to

monitor the large monovalent current. The monovalent current did not decline in parallel with I_{CRAC}, but instead grew progressively larger over 400 s (Fig. 3 A, right). A plot of the time courses of the Ca^{2+} current and the Na^+ current in this cell shows clearly that the amplitude of the large Na^+ current increases even as CRAC channels close (Fig. 3 B). Similar results were observed in 5/5 cells. Together with the changes in ion selectivity and kinetic behavior noted above, these results argue strongly that the large monovalent current arises from store-independent channels distinct from the CRAC channel.

The Large Monovalent Current and I_{CRAC} Have Different Pharmacological Profiles

To further establish differences between the large monovalent current and CRAC channels and find conditions that could be used to isolate each current, we compared their sensitivities to SKF 96365 and 2-APB. SKF 96365 is an imidazole antimycotic compound that inhibits CRAC channels and several other SOCs with IC_{50} values of 0.6–16 μM (Franzius et al., 1994; Christian et al., 1996a). Application of 20 μM SKF 96365 caused robust and partially reversible inhibition of I_{CRAC} (Fig. 4 A). On average, the peak current amplitude was diminished by 87 ± 4% with a time constant of 17 ± 7 s ($n = 6$). In contrast, the same concentration of SKF 96365 had very little effect on the large monovalent current (Fig. 4 B), inhibiting by only 10 ± 2% after 120 s of exposure ($n = 4$). Two results argue that the resistance of the monovalent current to block by SKF 96365 is not due to DVF conditions per se. First, with 20 mM Ca^{2+} present, the compound also failed to inhibit the outwardly rectifying current seen in Fig. 2 D, which we believe is mediated by the same channels that conduct the large monovalent current under DVF conditions (see below). Furthermore, complete inhibition of I_{CRAC} by drug application in the presence of Ca^{2+} did not affect or delay the appearance of the large monovalent current upon removal of extracellular divalents (Fig. 4 C). Thus, CRAC channels and the large monovalent current are distinctly different in their sensitivities to inhibition by SKF 96365.

A comparison of the effects of 2-APB provides further evidence that the two currents are distinct. 2-APB, originally described as a noncompetitive antagonist of IP_3 receptors, also inhibits store-operated Ca^{2+} entry in several cell types (Ma et al., 2000; Broad et al., 2001; Prakriya and Lewis, 2001). We have shown previously that I_{CRAC} in Jurkat cells is enhanced several-fold by low concentrations of 2-APB (≤5 μM) and that this potentiation is followed by nearly irreversible inhibition at higher concentrations (IC_{50} of ~10 μM) (Prakriya and Lewis, 2001). The dual effects of 2-APB are illustrated in Fig. 5, which shows potentiation of I_{CRAC} by 5 μM 2-APB (Fig. 5 A), and potentiation and subsequent inhibition by 50 μM 2-APB (Fig. 5 B). The large monova-

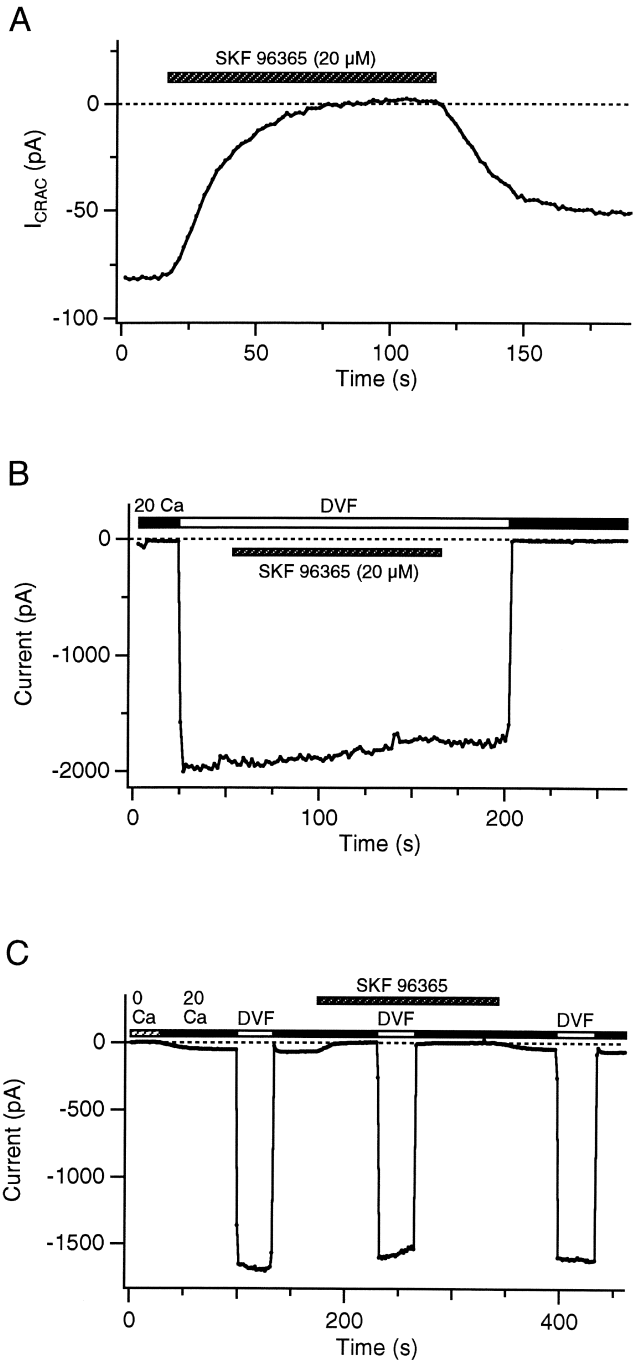

FIGURE 4. I_{CRAC} and the large monovalent current exhibit different sensitivities to SKF 96365. All cells were pretreated with 1 μM TG. In B and C, the recordings began after the monovalent current had activated to a steady-state level, as described in Fig. 2. Both currents were measured during steps to −110 mV. (A) Inhibition of I_{CRAC} by SKF 96365 (20 μM). Inhibition and recovery followed exponential time courses with time constants of 17.5 and 19 s, respectively. Internal solution: Cs methanesulfonate/10 BAPTA/8 Mg^{2+}. External: 20 mM Ca^{2+}. (B) The large monovalent current is relatively insensitive to 20 μM SKF 96365. Internal solution: MGF. (C) Even after nearly complete inhibition of I_{CRAC} by SKF 96365 (20 μM), removal of external divalent ions causes the monovalent current to rise rapidly to control levels. Thus, the insensitivity of the monovalent current to SKF 96365 is not explained by a failure to block CRAC channels under DVF conditions. Internal solution: MGF.

lent current differed dramatically in its response to 2-APB. First, low concentrations of 2-APB (≤5 μM) failed to enhance the large monovalent current. Second, 50 μM 2-APB inhibited the large monovalent current by <50% (Fig. 5 C). In six cells, 40 μM 2-APB inhibited I_{CRAC} by 97 ± 2% (Prakriya and Lewis, 2001), but inhibited the large Na^+ current by only 48 ± 6%. Inhibition by 50 μM 2-APB of the large monovalent current was also much slower (τ = 90 ± 8 s; n = 6) than inhibition of I_{CRAC} (τ = 10 ± 1 s, n = 6; Prakriya and Lewis, 2001). Finally, inhibition of the large Na^+ current was rapidly and completely reversible, whereas block of I_{CRAC} was essentially irreversible (see Fig. 5 B; Prakriya and Lewis, 2001). Thus, the large monovalent current and I_{CRAC} exhibit clearly different sensitivities and responses to 2-APB.

The Large Monovalent Current Is Normal in Mutant Jurkat Cells Lacking I_{CRAC}

We also tested for the presence of the large monovalent current in Jurkat cell mutants that express low levels of I_{CRAC}. One of these lines, CJ-2, expresses ~14% of the normal level of I_{CRAC} (Fanger et al., 1995). Despite this defect in store-operated Ca^{2+} entry, CJ-2 cells express normal levels of I_{MIC} (−114 ± 8 pA/pF [n = 5] in CJ-2 vs. −127 ± 23 pA/pF [n = 7] in wild-type cells; measured at −110 mV). These results provide genetic evidence that CRAC channels and the large monovalent current represent distinct conduction pathways.

In sum, multiple independent lines of evidence demonstrate that the large monovalent current evoked in the absence of extracellular divalent ions and intracellular Mg^{2+} does not flow through CRAC channels. The large monovalent current is not store-dependent, its time course is independent of changes in CRAC channel activity, it is pharmacologically distinct from I_{CRAC} and its expression is regulated independently of CRAC in mutant cells. In the following section we examine the properties of the large monovalent conductance and describe methods for inhibiting it so that monovalent currents through CRAC channels can be measured in isolation.

The Large Monovalent Current Is Inhibited by Intracellular Mg^{2+}

The induction of the large monovalent current by intracellular pipette solutions lacking Mg^{2+} suggests that it may be activated as intracellular Mg^{2+} is dialysed out of the cell. We obtained direct support for this idea at both the whole-cell and single-channel levels. Addition of 8 mM $MgCl_2$ to the whole-cell pipette solution completely suppressed the activation of the large monovalent current under DVF conditions (Fig. 6 A) with an IC_{50} of ~0.6 mM (Fig. 6 B). Intracellular Mg^{2+} also inhibited the development of the outwardly rectifying current seen in 20 mM $Ca^{2+}{}_o$ (Fig. 2 D) with about the

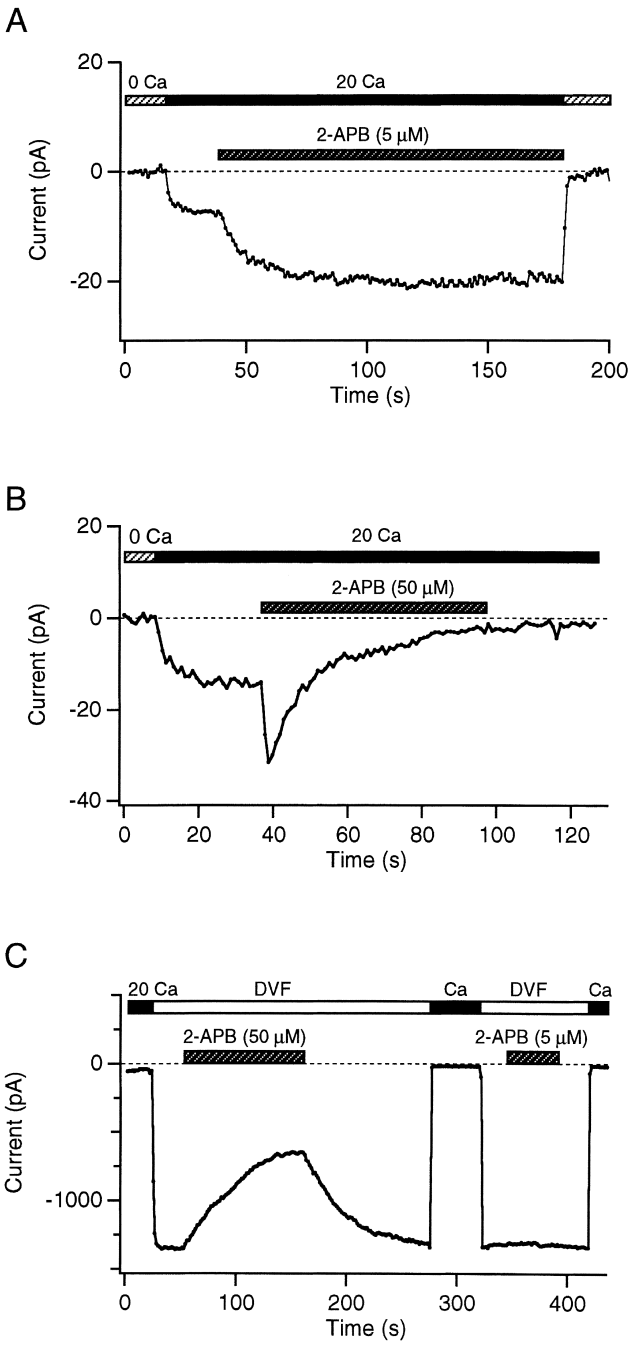

FIGURE 5. I_{CRAC} and the large monovalent current have differing sensitivities to 2-APB. (A) A low concentration of 2-APB (5 μM) enhances I_{CRAC} after full store depletion by TG. I_{CRAC} is shown at −110 mV. Internal solution: Cs methanesulfonate/10 BAPTA/8 Mg^{2+}. Holding potential: −40 mV (B) A high concentration of 2-APB (50 μM) initially enhances, then produces nearly complete and irreversible inhibition of I_{CRAC}. Experimental conditions as described in A. (C) Effects of 2-APB on the large monovalent current. A high concentration (50 μM) inhibits the current partially and reversibly. In contrast, the irreversible inhibition of I_{CRAC} in the same cell is shown by comparing currents during the first and second applications of Ca^{2+}. 5 μM 2-APB fails to enhance the large monovalent current, although it enhances I_{CRAC} as shown in A. Internal solution: MGF.

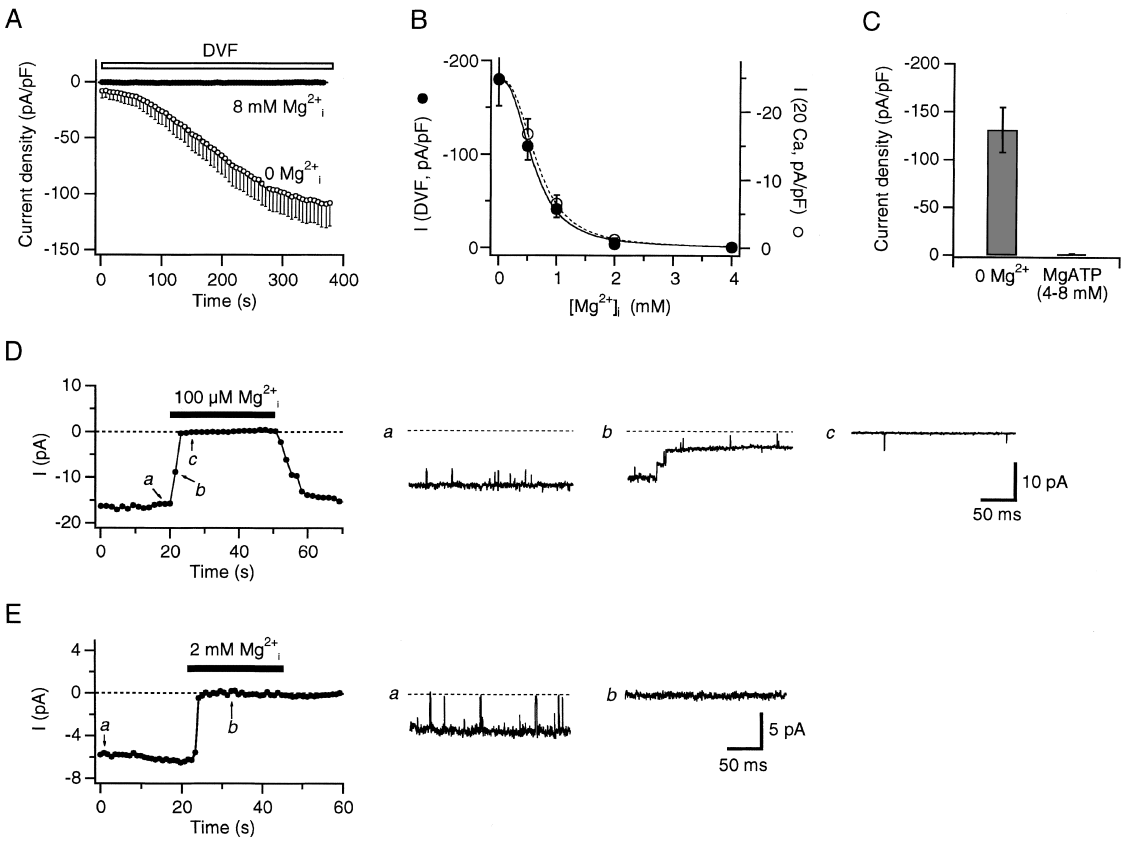

FIGURE 6. The large monovalent current is inhibited by intracellular Mg^{2+} and MgATP. (A) High intracellular [Mg^{2+}] prevents activation of the large monovalent current. Mean currents at −110 mV in the presence of DVF Ringer's are shown as a function of time following break-in. Internal solution: Cs methanesulfonate containing either 10 HEDTA/0 Mg^{2+} (○; six cells) or 10 BAPTA/8 mM Mg^{2+} (●; four cells). (B) Dose-response curves for Mg^{2+}-dependent inhibition of the inward Na^+ current (●) recorded at −110 mV in DVF solution and the outward Cs^+ current (○) at 90 mV in 20 mM $Ca^{2+}{}_o$ solution. The two extracellular solutions were periodically alternated as described in Fig. 2. Each point represents the mean ± SEM of 5–7 cells. The solid and dotted lines are fits of the equation $I = 1/(1 + ([Mg^{2+}]/K_{1/2})^n)$ with the following parameter values: $K_{1/2} = 0.6$ mM and $n = 2.4$ for the inward current in DVF; $K_{1/2} = 0.66$ mM and $n = 2.6$ for the outward current in 20 mM $Ca^{2+}{}_o$. Internal solution: Cs methanesulfonate/10 mM BAPTA containing indicated levels of calculated free Mg^{2+}. (C) The large monovalent current is inhibited by intracellular MgATP. Shown are the mean whole-cell current amplitudes 400 s after break-in with internal solutions containing 4–8 mM MgATP (five cells) or 0 Mg^{2+}/10 HEDTA (six cells), in experiments like the one shown in A. (D) Reversible inhibition of MIC channels by 100 μM $Mg^{2+}{}_i$ in excised patches. Channel activity persisted in this inside-out patch after excision into MGF solution. Application of 100 μM Mg^{2+} (free concentration, buffered with 10 mM HEDTA) to the cytoplasmic face resulted in reversible closure of two channels. The average current amplitudes during 250-ms steps to −115 mV are shown, with selected sweeps shown at higher time resolution to the right (dashed line indicates 0 current level). Pipette solution: Na-DVF. (E) 2 mM Mg^{2+} inhibits single-channel monovalent currents irreversibly. Same conditions as in D, except 2 mM Mg^{2+} was applied with 10 mM BAPTA.

same efficacy (Fig. 6 B), suggesting that both currents arise from the same channel.

Mg^{2+} applied to the cytoplasmic side also inhibited single-channel monovalent currents in excised inside-out patches. An intriguing feature of Mg^{2+}-inhibition of these channels in excised patches was that full inhibition was observed even at Mg^{2+} concentrations as low as 100 μM (Fig. 6 D; 3/3 patches). At present, we do not understand why the sensitivity to Mg^{2+} increases after patch excision. Unlike the effect of 100 μM Mg^{2+}, application of 2 mM Mg^{2+} to the cytoplasmic face of the membrane caused irreversible channel closure (Fig. 6 E; 8/8 patches). Similar effects have been reported for the 40-pS channels in RBL cells (Braun et al., 2001). The slow time course and variable reversibility of inhibition by Mg^{2+} suggests that Mg^{2+} causes channel closure rather than acting as a pore blocker. To denote their Mg^{2+} sensitivity and nonselective cation permeability, we refer to these channels as Mg^{2+}-inhibited cation channels (MICs), and to the whole-cell current as I_{MIC}. We apply this name for simplicity, and not to imply that intracellular Mg^{2+} is a physiological regulator of channel activity (see DISCUSSION).

To isolate I_{MIC} for further characterization, I_{CRAC} was blocked irreversibly by pretreatment with 100 μM 2-APB for 15 min. Following break-in with a Mg^{2+}-free internal solution, ramp currents were recorded while switching between 20 mM Ca^{2+} and DVF Ringer's solutions. Under these conditions, I_{MIC} (observed during brief applications of DVF Ringer's) developed in paral-

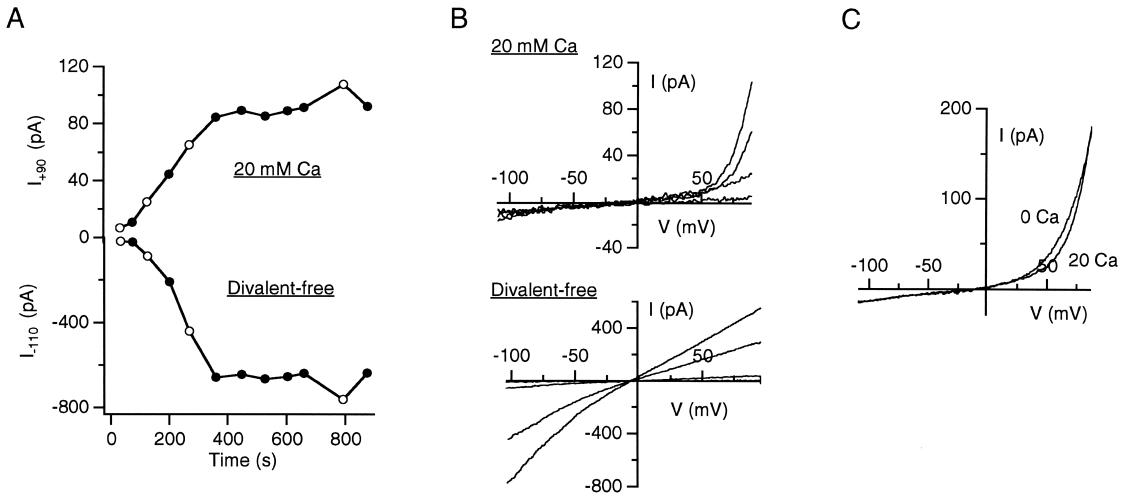

FIGURE 7. Effects of extracellular divalent cations on MIC current. The cell was treated with 100 μM 2-APB for 15 min before seal formation to irreversibly inhibit I_{CRAC}. Data are not corrected for leak current. Internal solution: MGF. Extracellular solution was alternated between 20 mM Ca^{2+} and DVF Ringer's as currents were measured in response to voltage ramps from −110 to 90 mV. (A) Parallel activation of inward Na^+ current at −110 mV (measured in DVF Ringer's) and outward Cs^+ current at 90 mV (measured in 20 mM Ca^{2+}_o). (B) Ramp currents collected at the times shown by the open symbols in A. The similar activation time courses of the currents in 20 mM Ca^{2+} and DVF conditions (shown in A) suggest that the outwardly rectifying currents in 20 mM Ca^{2+} are due to MIC channels. (C) Removal of extracellular Ca^{2+} (2 mM Mg^{2+}_o) does not alter the inward MIC current.

lel with an outwardly rectifying current (observed during applications of 20 Ca^{2+} Ringer's) (Fig. 7, A and B). Similar behavior was seen in 5/5 cells. As with I_{MIC}, the outwardly rectifying current was not observed when 8–10 mM Mg^{2+} was included in the pipette solution (unpublished data), supporting the idea that this current is conducted by MIC channels.

Under DVF conditions, MIC currents reverse at -6 ± 2 mV ($n = 5$), indicating a P_{Cs}/P_{Na} ratio of 1.2. In the presence of extracellular divalent ions, however, the permeability of MIC channels is complex. Addition of divalent ions transforms the linear I-V relation in DVF conditions to a outwardly rectifying one, suggesting that external divalent ions block monovalent current flow in a voltage-dependent manner. I_{MIC} reverses around 0 mV under these conditions also (Fig. 7), consistent with a lack of selectivity among cations. Our preliminary results from ion substitution experiments indicate that Na^+, Ca^{2+}, and Mg^{2+} all carry current through MIC channels at negative potentials; however, Mg^{2+} and Ca^{2+} also block the passage of Na^+, making it difficult on the basis of ion substitution experiments to determine the exact proportion of current carried by each ionic species. For this reason, we did not characterize the permeation properties of MIC channels further, but instead focused on ways to prevent contamination of I_{CRAC} measurements with I_{MIC}. Importantly, the inward MIC current is unaffected by switching from 20 mM Ca^{2+}_o to a Ca^{2+}-free Ringer's solution containing 2 mM Mg^{2+} (Fig. 7 C). Therefore, for purposes of isolating I_{CRAC} at negative potentials, leak subtraction using currents obtained in a Ca^{2+}-free solution effectively removes the contaminating current arising from MIC channels (see MATERIALS AND METHODS).

A recently cloned member of the TRP family of ion channels, called TRP-PLIK (Runnels et al., 2001) or LTRPC7 (Nadler et al., 2001), has an ionic selectivity and current-voltage relation quite similar to that of MIC. LTRPC7 is expressed in Jurkat cells and is inhibited by intracellular Mg^{2+} as well as by intracellular MgATP (Nadler et al., 2001). Likewise, we found that MgATP at concentrations of 4 mM and higher in the intracellular pipette solution completely inhibited the development of I_{MIC} (Fig. 6 C), whereas recordings with 3 mM MgATP exhibited sporadic MIC channel activity. Our combined observations suggest that I_{MIC} is mediated by TRP-PLIK/LTRPC7 channels, and is probably identical to an outwardly rectifying MgATP-sensitive current (called MagNuM, for Mg^{2+} nucleotide–regulated metal) that has been reported in Jurkat, RBL, and HEK293 cells (Nadler et al., 2001).

Isolating the Monovalent Current through CRAC Channels

Inhibition of I_{MIC} by intracellular Mg^{2+} offers a convenient strategy for isolating the monovalent current through CRAC channels for characterization. With 8 mM intracellular Mg^{2+} to suppress I_{MIC}, passive depletion of Ca^{2+} stores by intracellular BAPTA (10 mM) slowly evoked I_{CRAC} in the presence of 20 mM Ca^{2+} (Fig. 8 A). Periodic exposure to DVF solution revealed a monovalent current which developed with the same time course as I_{CRAC} (Fig. 8 B). Similar results were seen

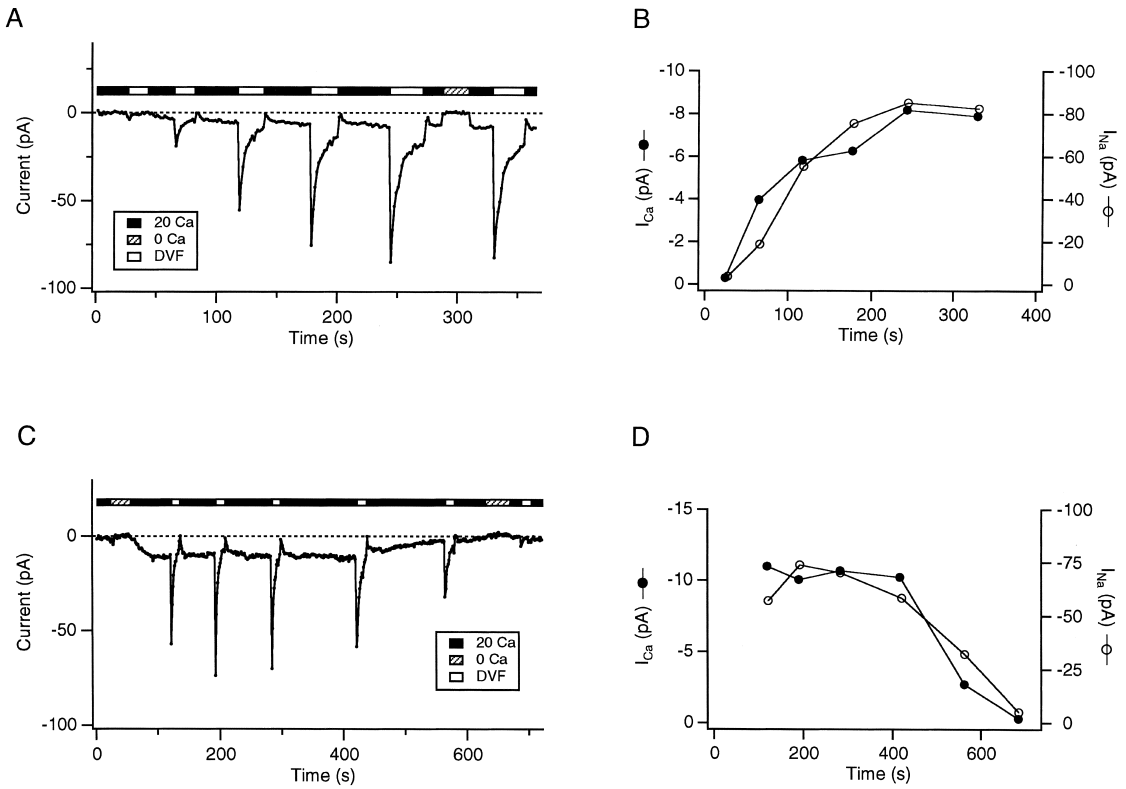

FIGURE 8. Activation and deactivation of Ca^{2+} and Na^+ currents through CRAC channels. Currents were measured during steps to −110 mV. (A) Activation of I_{CRAC} and the transient Na^+ current during passive store depletion with a pipette solution containing 10 mM BAPTA + 8 mM Mg^{2+}. Periodic removal of external divalent ions reveals a transient monovalent current that increases in parallel with I_{CRAC}. (B) The Ca^{2+} current (●) and the peak Na^+ current (○) measured immediately before and during each application of DVF solution activate with similar kinetics. (C) Deactivation of I_{CRAC} and the transient monovalent current during intracellular dialysis with 1 mM BAPTA + 8 mM Mg^{2+}. As described in Fig. 3 A, I_{CRAC} deactivates in the presence of low intracellular Ca^{2+} buffering, presumably due to store refilling. (D) The Ca^{2+} current (●) and the peak Na^+ current (○) decline in parallel in the experiment in C. The similar activation and deactivation kinetics for the Na^+ and Ca^{2+} currents support the idea that the transient monovalent current represents Na^+ flux through CRAC channels.

in 7/7 cells. The monovalent current was transient during each DVF episode, peaking immediately after solution exchange and subsequently declining with a time constant of ~10 s. The ratio of the peak amplitude of the Na^+ current to I_{CRAC} measured just before solution exchange was 7.8 ± 0.4 (n = 17).

The parallel activation kinetics of I_{CRAC} and the transient monovalent current suggests that the latter current represents flux through CRAC channels. As a further test, we examined the transient monovalent current's dependence on store refilling under conditions that inhibit I_{MIC} activation (8–10 mM $Mg^{2+}{}_i$). In the presence of 1 mM intracellular BAPTA and 20 mM $Ca^{2+}{}_o$, activation of I_{CRAC} was followed by characteristic slow deactivation, presumably as Ca^{2+} entering the cell overwhelmed the buffer and refilled the stores (Zweifach and Lewis, 1995) (Fig. 8 C). Periodic removal of external divalents showed that the transient Na^+ current decreased in parallel with I_{CRAC} (Fig. 8, C and D). Similar behavior was seen in 6/6 cells. Together, these results show that the transient Na^+ current is store-dependent, similar to I_{CRAC} but unlike I_{MIC}.

The pharmacological profile of the transient Na^+ current also closely matched that of I_{CRAC}. As shown in Fig. 9 A, 20 μM SKF 96365 inhibited both currents to similar extents. On average, I_{CRAC} was reduced by 84 ± 3% (n = 4), whereas the inactivating Na^+ current was reduced by 74 ± 3% in the same cells. Moreover, 5 μM 2-APB potentiated both currents, enhancing I_{CRAC} by 241 ± 41% (n = 7) and the peak amplitude of the transient Na^+ current in the same cells by 185 ± 31% (Fig. 9 B). 2-APB also enhanced the steady-state component of the Na^+ current by a similar amount (224 ± 26%; n = 6). These results suggest that the residual current remaining after the Na^+ current has declined is also due to CRAC channels, a conclusion that is consistent with the observation that the peak and the residual currents reverse at the same potential (see below).

High concentrations of 2-APB inhibited the transient Na^+ current as they did I_{CRAC}. As illustrated in Fig. 9 C, 40 μM 2-APB was applied to irreversibly inhibit I_{CRAC}, and the transient Na^+ current was measured under DVF conditions following washout of the drug. In three cells, 50 μM 2-APB reduced I_{CRAC} in the presence of 20

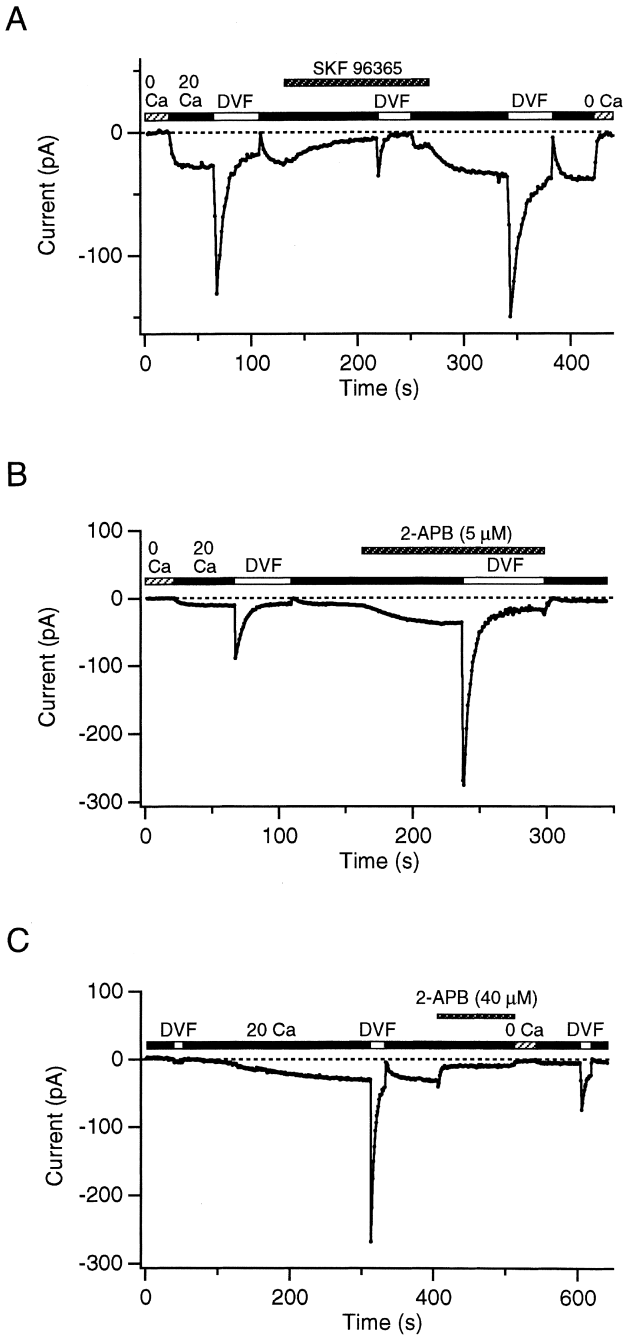

FIGURE 9. Pharmacological evidence for monovalent currents through CRAC channels. I_{CRAC} was activated by treatment with 1 μM TG for 5 min before seal formation (in A and B) or by passive depletion with 10 mM intracellular BAPTA (in C), with 10 mM intracellular Mg^{2+} to inhibit I_{MIC}. (A) SKF 96365 (20 μM) inhibits both I_{CRAC} and the transient monovalent current (under DVF conditions). Both currents recover following washout of the drug. (B) A low concentration of 2-APB (5 μM) enhances both I_{CRAC} and the transient monovalent current by severalfold. (C) A high concentration of 2-APB (40 μM) significantly reduces both I_{CRAC} and the transient monovalent current. The inhibition of both currents persists after washout of the drug.

mM Ca^{2+} by 83 ± 3% and the monovalent current by 80 ± 6%. These results also show that block of the transient monovalent current by 2-APB outlasts bath application of the drug, as is the case for I_{CRAC} but not I_{MIC} (Fig. 5). Thus, the pharmacological properties of the transient Na^+ current are consistent with those of I_{CRAC}.

Based on these results as well as the evidence given above that I_{CRAC} and the transient Na^+ current activate and deactivate in parallel and are store-dependent, we conclude that 8–10 mM intracellular Mg^{2+} suffices to isolate the monovalent current through CRAC channels in the absence of extracellular divalent ions. For convenience, the inward Na^+ and Ca^{2+} currents through CRAC channels will hereafter be referred to as Na^+-I_{CRAC} and Ca^{2+}-I_{CRAC}, respectively.

The Monovalent Selectivity of CRAC Channels Is Not Influenced by Intracellular Mg^{2+}

The identification of a Mg^{2+}-sensitive monovalent current raises new questions about the possible role of Mg^{2+} in shaping the properties of CRAC channels. Previous studies have concluded that intracellular Mg^{2+} blocks permeation of Cs^+ through CRAC channels under DVF conditions (Kerschbaum and Cahalan, 1998). Using the methods described above for separating I_{MIC} from I_{CRAC}, we reassessed the role of Mg^{2+} in CRAC channel selectivity.

Fig. 10 A shows the transient monovalent CRAC current with 8 mM $Mg^{2+}{}_i$ and with equimolar Cs^+ and Na^+ as the principal intracellular and extracellular cations, respectively. The I-V relations recorded as the current depotentiated show pronounced inward rectification and intersect at a single potential. This supports the idea that the whole-cell current decreases due to the closure of a single channel type, i.e., CRAC channels, and that the residual steady-state current is also due to CRAC channels as discussed above. The crossover point in eight cells was 52 ± 2 mV, implying that CRAC channels under DVF conditions are only weakly permeable to Cs^+ (P_{Cs}/P_{Na} = 0.13 based on the Goldman-Hodgkin-Katz equation). A similar reversal potential was obtained from single ramp currents after subtraction of leak current recorded in 0-Ca Ringer's (unpublished data). Thus, unlike MIC channels, CRAC channels in the absence of divalent cations select strongly against Cs^+ (compare Fig. 7 B). Consistent with this conclusion, replacement of extracellular Na^+ with Cs^+ eliminates nearly all of the inward monovalent current through CRAC channels (Fig. 10 B).

These experiments do not address the role of Mg^{2+} in determining the selectivity against Cs^+, because 8–10 mM intracellular Mg^{2+} was present to block I_{MIC}. Unfortunately, if intracellular Mg^{2+} is removed, I_{MIC} develops to such an extent that it readily swamps the small monovalent current through CRAC channels. There-

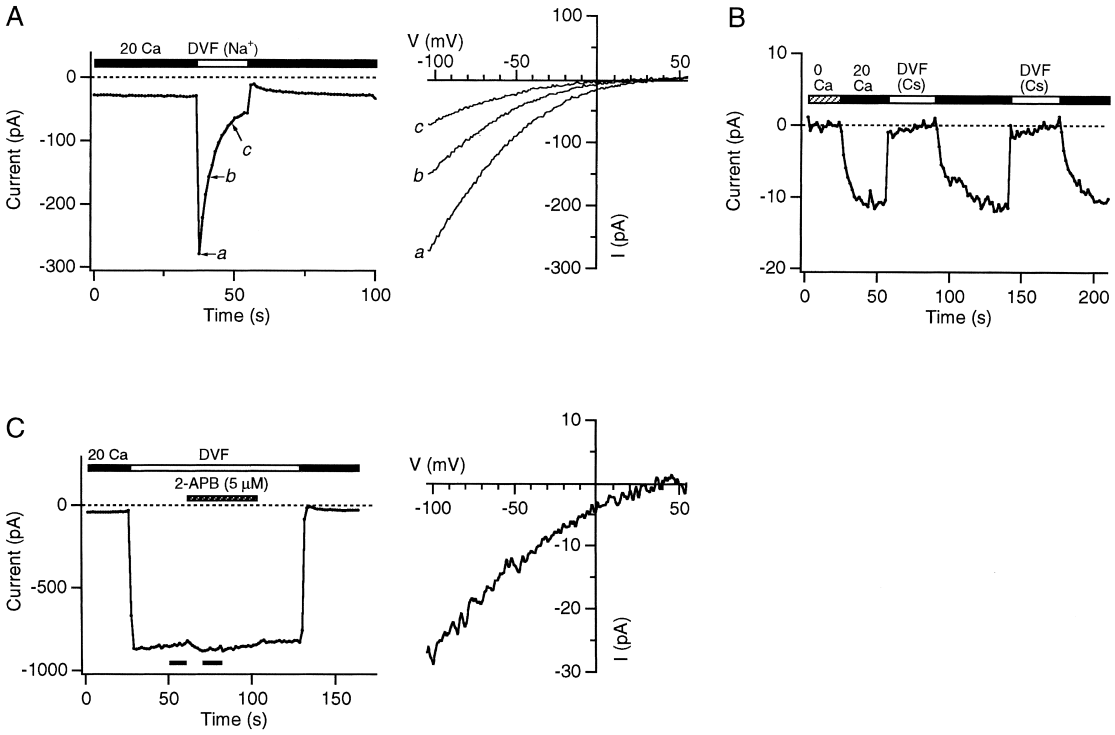

FIGURE 10. CRAC channels have a low permeability to Cs^+. I_{CRAC} was activated by treatment with 1 μM TG, and measured in response to steps to −110 mV and ramps from −110 to 50 mV. (A) Positive reversal potential of monovalent CRAC current with Cs^+ and Na^+ as the primary intracellular and extracellular current carriers, respectively. Three ramp currents collected during the depotentiation of Na^+-I_{CRAC} (left graph) converge at ~50 mV (right). (A and B) Internal solution: Cs methanesulfonate/10 BAPTA/8 Mg^{2+}. (B) Extracellular Cs^+ does not conduct significant inward current through CRAC channels under DVF conditions. When the bath solution is changed to a Cs^+-based DVF solution, the current at −110 mV drops to ~15% of its previous value in 20 mM Ca^{2+}; in contrast, Na^+-DVF causes an approximately eightfold increase in the current. Thus, Na^+ is ~50-fold more conductive than Cs^+. (C) Measurement of the CRAC-channel current-voltage relation under DVF conditions in the absence of intracellular Mg^{2+}. A low concentration of 2-APB (5 μM) induces an inward current that sums with I_{MIC}. Ramp currents were averaged before and after 2-APB treatment (bars). Because 2-APB selectively enhances CRAC channel activity (Fig. 5), the difference between the two averaged currents isolates monovalent I_{CRAC} (right). The net current reverses at ~40 mV, indicating that the low Cs^+ permeability of the CRAC channel is independent of intracellular Mg^{2+}. Internal solution: MGF.

fore, to measure Na^+-I_{CRAC} in the absence of Mg^{2+}, we exploited the ability of 2-APB to enhance I_{CRAC} selectively. After the full development of I_{MIC} with 0 $Mg^{2+}{}_i$, 5 μM 2-APB was applied to elevate I_{CRAC}. The current immediately before 2-APB application was subtracted from the enhanced current to remove the contribution of I_{MIC} (Fig. 10 C). The I-V relation of the additional monovalent current is similar to that of the current recorded in the presence of 8 mM $Mg^{2+}{}_i$ (Fig. 10 A). The 2-APB-enhanced current reverses at potentials >40 mV and shows inward rectification, though to a slightly lesser extent than in the presence of $Mg^{2+}{}_i$ (compare Fig. 10 C with 10 A). Thus, the low permeability of CRAC channels to Cs^+ does not require intracellular Mg^{2+}, but is instead likely to be an intrinsic property of the CRAC channel pore.

Depotentiation of CRAC Channels Is Independent of Intracellular Mg^{2+}

The activity of CRAC channels slowly declines by up to 80% after removal of extracellular Ca^{2+}, and recovers over 10–20 s after its reapplication by a process referred to as Ca^{2+}-dependent potentiation, or CDP (Christian et al., 1996b; Zweifach and Lewis, 1996). Thus, the current's decline following the removal of extracellular divalents reflects depotentiation. Previous findings that transient monovalent currents (thought to be through CRAC channels) became large and sustained in the absence of intracellular Mg^{2+} led to the suggestion that internal Mg^{2+} is required for the depotentiation process, and that CDP may arise from the expulsion of Mg^{2+} ions from the pore of CRAC channels by permeant Ca^{2+} ions (Kerschbaum and Cahalan, 1998). Because I_{MIC} was likely mistaken for I_{CRAC} in the absence of intracellular Mg^{2+}, we reexamined the role of Mg^{2+} in CRAC channel depotentiation under conditions that prevent activation of I_{MIC}.

To effectively inhibit I_{MIC} under conditions of low intracellular Mg^{2+}, we applied MgATP in combination with Na_2ATP to reduce free $[Mg^{2+}]_i$. 6–8 mM MgATP + 2–6 mM Na_2ATP in the pipette solution inhibited I_{MIC} while reducing free $[Mg^{2+}]_i$ to calculated values of

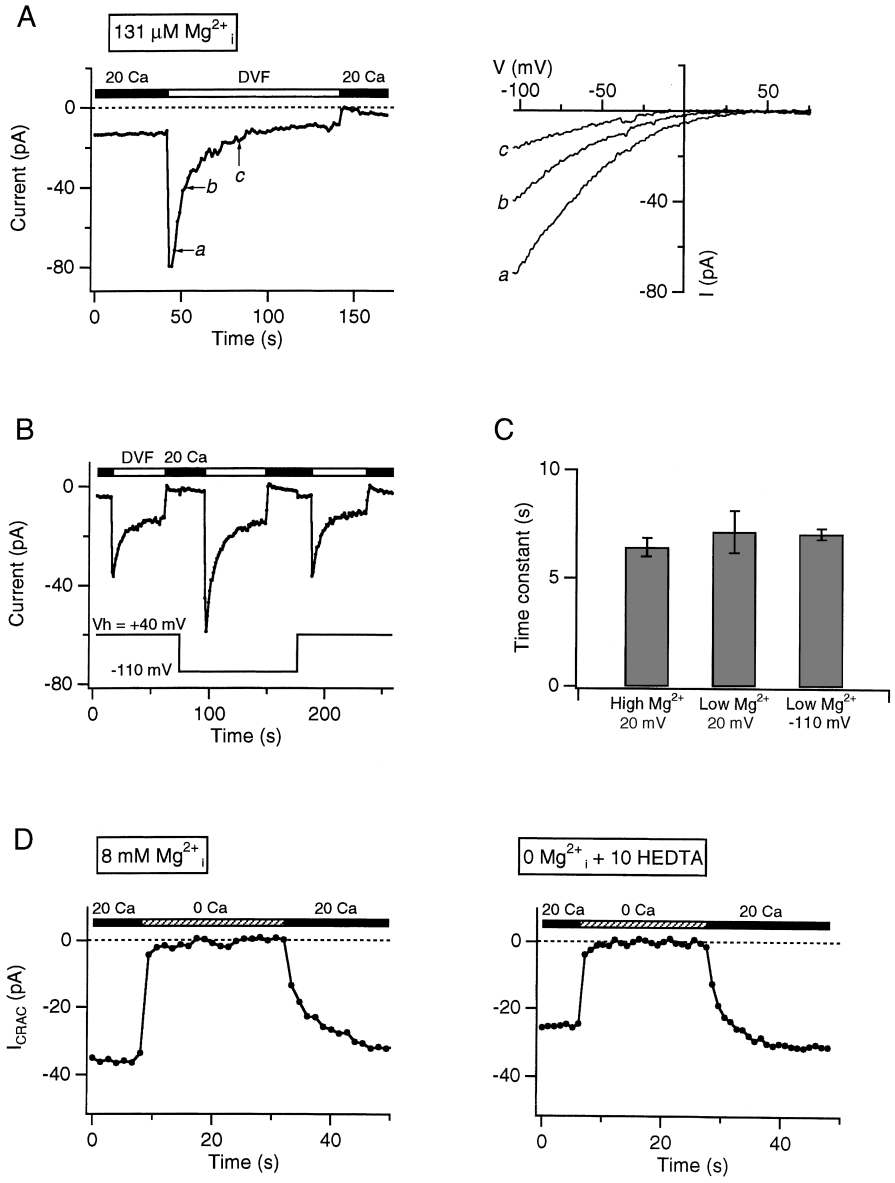

FIGURE 11. Intracellular Mg^{2+} is not involved in the depotentiation of CRAC channels following removal of extracellular Ca^{2+}. I_{CRAC} was activated by treatment with 1 μM TG, and currents were measured at a step potential of −110 mV. (A) Depotentiation of Na^+-I_{CRAC} occurs even in the presence of low cytoplasmic [Mg^{2+}]. The pipette solution contained 8 mM MgATP to inhibit I_{MIC} and 6 mM Na_2ATP to reduce free [Mg^{2+}] to 131 μM (calculated). Ramp currents collected at several times during the decline of Na^+-I_{CRAC} are shown at the right. (B) The kinetics of Na^+-I_{CRAC} decline are not voltage dependent. Transient Na^+-I_{CRAC} was evoked by exposure to DVF solution at a holding potential of 40 or −110 mV, with the same intracellular solutions as in A. The peak amplitude of Na^+-I_{CRAC} (measured during steps to −110 mV) is larger at the more negative holding potential, presumably due to the voltage dependence of CDP (see Zweifach and Lewis, 1996). However, the extent and rate of depotentiation are unaffected. (C) The rate of depotentiation is unaffected by the level of $[Mg^{2+}]_i$ or membrane potential. Exponential curves were fitted to the depotentiation time course with 8 mM $Mg^{2+}{}_i$ at 20 mV (seven cells), 90–131 μM $Mg^{2+}{}_i$ at 20 mV (7 cells), or 131 μM Mg^{2+} at −110 mV holding potential (three cells). (D) Removal of intracellular Mg^{2+} does not affect CDP. After exposure to Ca^{2+}-free conditions, readdition of extracellular Ca^{2+} causes I_{CRAC} to reappear gradually over 10–20 s due to CDP. The extent and time course of CDP were similar in experiments with 8 mM $Mg^{2+}{}_i$ (left) or 0 $Mg^{2+}{}_i$ (right). Holding potential, 20 mV.

~92–185 μM (see MATERIALS AND METHODS). Under these conditions, Na^+-I_{CRAC} still depotentiated after removal of extracellular divalents (Fig. 11 A), and the I-V relationship of the current was similar to that recorded with 8 mM $Mg^{2+}{}_i$. Neither the time course (Fig. 11 C) nor the amplitude of depotentiation were altered relative to cells with 8 mM $Mg^{2+}{}_i$; the fraction of current remaining after 50 s of DVF application was 20 ± 4% (n = 7) with 131 μM $Mg^{2+}{}_i$ vs. 18 ± 2% (n = 8) with 8 mM $Mg^{2+}{}_i$. Finally, if depotentiation were to arise from Mg^{2+} binding in the pore of the CRAC channel and within the membrane field, hyperpolarization would be expected to inhibit it by reducing Mg^{2+} binding. However, shifting the holding potential from 40 mV to −110 mV did not significantly alter the rate of depotentiation at either high (6–10 mM) or low (131 μM) levels of $Mg^{2+}{}_i$ (Fig. 11, B and C), even though the maximum amplitude of Na^+-I_{CRAC} was increased, consistent with the voltage dependence of CDP (Zweifach and Lewis, 1996). Together, these results argue against a necessary role for intracellular Mg^{2+} in the depotentiation of CRAC channels.

However, an alternative explanation could be that the putative Mg^{2+} site for depotentiation has a high affinity and does not lie within the membrane field. We examined this possibility by exploring Mg^{2+} effects on Ca^{2+}-I_{CRAC}. Full removal of intracellular Mg^{2+} in the presence of extracellular Ca^{2+} evokes only a small inward I_{MIC}, and the current is not affected by removal of $Ca^{2+}{}_o$ alone (Fig. 7 C), providing a way of isolating it from I_{CRAC} through leak subtraction. Therefore, we used these conditions to ask whether Ca^{2+}-I_{CRAC} depotentiates in the absence of intracellular Mg^{2+}. Depotentiation of I_{CRAC} in the absence of $Ca^{2+}{}_o$ can be detected

indirectly by the slow recovery of full current amplitude after readdition of Ca^{2+} (Fig. 11 D). Under control conditions (8 mM Mg^{2+}_i), Ca^{2+} readdition causes Ca^{2+}-I_{CRAC} to appear in two kinetically distinct stages: a small fraction of the current appears immediately (i.e., within the 2-s exchange time of the perfusion system) that represents the current through active CRAC channels, followed by a several-fold increase in current amplitude over the next 10–20 s due to CDP. Thus, the size of the slowly relaxing current component reflects the extent of depotentiation that occurred before the readdition of Ca^{2+}. Significantly, neither the amplitude nor the time course of CDP was affected by intracellular Mg^{2+}. At a holding potential of 20 mV, CDP caused a 104 ± 5% increase in Ca^{2+}-I_{CRAC} with an average τ of 2.9 ± 0.3 s ($n = 6$) in cells with 8 mM Mg^{2+}_i, and a 114 ± 7% increase with τ = 3.1 ± 0.4 s ($n = 4$) in cells in which Mg^{2+}_i was chelated by 10 mM HEDTA. These results are consistent with those of Figs. 2 and 3, where I_{CRAC} depotentiates during applications of DVF solution in the absence of Mg^{2+}_i. Thus, intracellular Mg^{2+} appears to have no influence on CRAC-channel depotentiation triggered by removal of extracellular Ca^{2+}.

Estimating the Unitary Na^+ Current through CRAC Channels by Noise Analysis

The finding that the 40-pS monovalent channels seen under DVF conditions are MIC channels raises new questions about the unitary monovalent conductance of CRAC channels. Under DVF conditions with 10 mM intracellular Mg^{2+} to inhibit I_{MIC}, we were unable to detect any clear single-channel transitions of amplitude >0.4 pA during the induction of Na^+-I_{CRAC} by ionomycin in 5/5 cells and during the or depotentiation of Na^+-I_{CRAC}. This contrasts with the obvious appearance of single-channel MIC currents when intracellular Mg^{2+} is washed out during whole-cell recording (Fig. 1). Therefore, we applied stationary fluctuation analysis to estimate the single-channel monovalent CRAC conductance.

Cells were treated with 1 μM TG to activate CRAC channels, and after establishing whole-cell recording the mean macroscopic current (I) and corresponding variance (σ_I^2) were measured at a holding potential of −110 mV. Application of 5 μM 2-APB enhanced I_{CRAC} in the presence of 20 mM Ca^{2+} and caused a barely detectable increase in current noise (Fig. 12 A). Subsequent removal of divalent cations (DVF conditions) evoked a transient Na^+ current through CRAC channels in parallel with a more robust increase in noise. Several 200-ms current sweeps used to compute the current mean and variance for the DVF condition are shown in Fig. 12 B, and indicate the lack of any clear single-channel transitions as the current declines. Plots of the current variance against mean current amplitude were well fitted by straight lines (Fig. 12, C and D). The average slope (σ_I^2/I) was −3.8 ± 0.6 fA ($n = 5$) in 20 mM Ca^{2+}, and −31 ± 2 fA ($n = 10$) under DVF conditions.

The relation of the variance to the mean current can be used to estimate the single-channel current given certain assumptions. For a homogeneous population of N independent channels with a single conducting level, i, stochastic gating predicts a parabolic relation between the current variance and the mean current as the open probability (P_o) varies between zero and one (Sigworth, 1980):

$$\sigma_I^2 = iI - \frac{I^2}{N} + \sigma_0^2,$$

where σ_0^2 is the variance at the zero-current level. Since $I = NiP_o$, it follows that

$$\frac{\sigma_I^2 - \sigma_0^2}{I} = i(1 - P_0). \quad (1)$$

Given these assumptions, the linear shape of the σ_I^2/I relation implies that the open probability of the channel is very low (<0.5) and that the unitary current amplitude is given by the slope (Eq. 1). Thus, the results would suggest that the unitary amplitude of monovalent I_{CRAC} at −110 mV is −31 fA; given the reversal potential of 52 mV, this corresponds to a single-channel chord conductance of ~0.2 pS.

There are several ways in which fluctuation analysis may seriously underestimate the unitary conductance. First, the bandwidth of the recording may not extend to high enough frequencies to capture the fluctuations due to very brief gating events. To test this, we analyzed the power spectrum of the current noise under DVF conditions. Fig. 12 E shows the background spectrum obtained in 0 Ca^{2+} + 2 mM Ni^{2+}, together with the spectrum of Na^+-I_{CRAC} at its peak and after it depotentiated to a steady level. In both cases, the noise approaches the background level at frequencies above ~1 kHz, suggesting that no large component of high-frequency noise was missed under the 1–2 kHz filtering conditions of the current variance experiments.

Second, noise measurements may underestimate the size of i if P_o is high and the macroscopic current amplitude reflects changes in N, the number of activatable channels, rather than P_o (Jackson and Strange, 1995). In this case, σ_I^2 will increase linearly with N:

$$\sigma_I^2 = Ni^2P_0(1 - P_0) + \sigma_0^2$$

and the σ_I^2/I ratio underestimates i by a factor of ($1 - P_o$) (Eq. 1). If this situation applies, a small reduction in the P_o resulting from extracellular blockade of the channels would be expected to produce an increase in channel noise due to an increased number of gating events occurring within each 200-ms sampling period. To examine this possibility, we added 1 μM free Ca^{2+} to

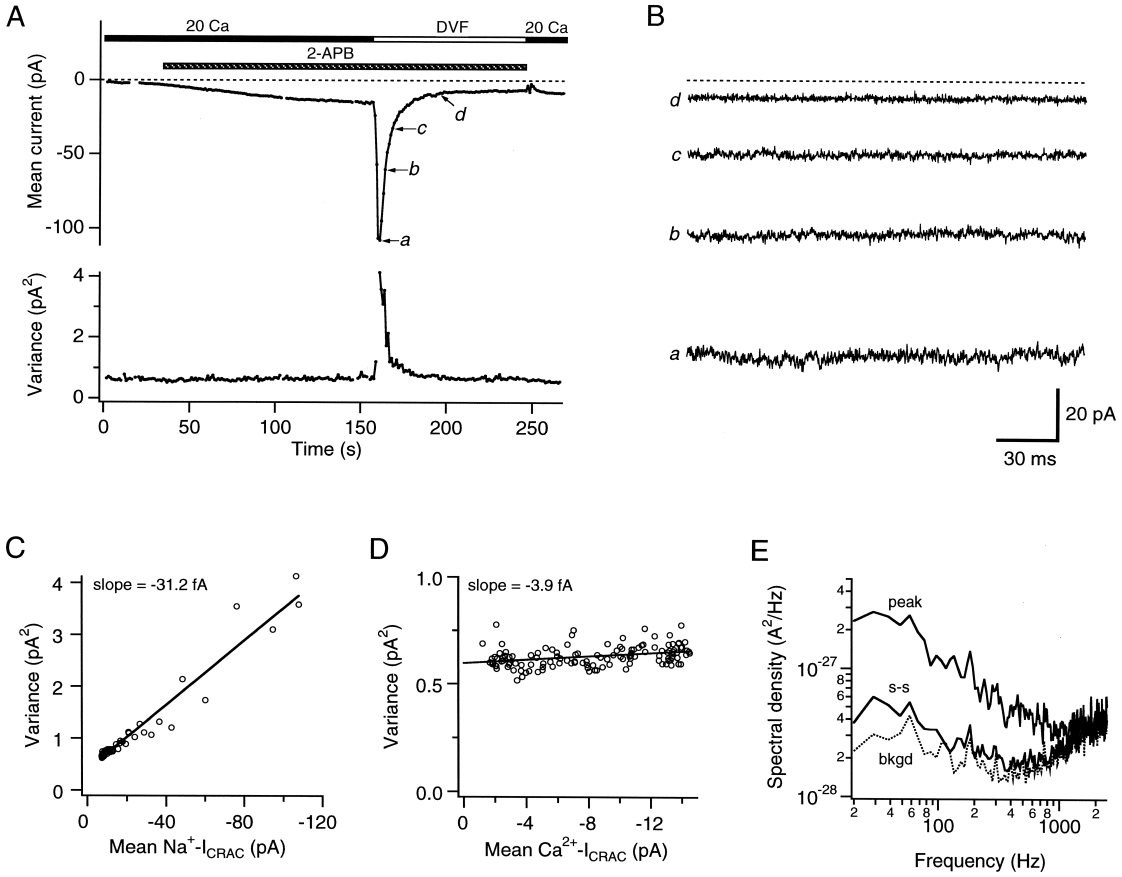

FIGURE 12. Fluctuation analysis of the Na^+ current through CRAC channels. I_{CRAC} was induced by treatment with 1 μM TG and was recorded at a constant holding potential of −110 mV. All data are from the same experiment. Internal solution: Cs methanesulfonate/10 BAPTA/8 Mg^{2+}. (A) Mean value and variance of CRAC current in response to 2-APB (5 μM) and removal of divalent cations. Each point represents the values calculated from a 200-ms segment of current data. (B) Sample 200-ms segments of Na^+-I_{CRAC} as it depotentiates in the presence of DVF Ringer's. The zero-current level is indicated by the dashed line. (C) Mean-variance analysis of Na^+-I_{CRAC}. The plot shows the mean value and variance of 200-ms current sweeps collected as Na^+-I_{CRAC} depotentiated in the presence of DVF Ringer's. The data points are well fit by a line with a slope of −31.2 fA. (D) Mean-variance analysis of Ca^+-I_{CRAC}. The plot shows the mean value and variance of 200-ms current sweeps collected as Ca^+-I_{CRAC} was enhanced by 2-APB in 20 mM Ca^{2+} Ringer's. The data points are well fit by a line with a slope of −3.9 fA. (E) Spectral analysis of Na^+-I_{CRAC}. Spectra were collected and averaged in 0 Ca^{2+} + 2 μM Ni^{2+} (dotted trace, "bkgd"), and near the peak of the transient Na^+ CRAC current ("peak") and after Na^+-I_{CRAC} reached steady-state ("s-s"). Each trace is the average of 3–20 spectra. There is little power above background levels associated with Na^+-I_{CRAC} at frequencies >1 kHz.

the extracellular DVF solution to partially block CRAC channels and reduce channel P_o. The peak I_{Na}/I_{Ca} ratio was reduced to 3.1 ± 0.3 (n = 4; versus a ratio of 7.8 ± 0.4 without the blocker), indicating >50% inhibition of the Na^+-I_{CRAC}. Under these conditions, the σ_I^2/I ratio was −19 ± 3 fA (n = 4). This ratio is even smaller than the σ_I^2/I ratios obtained in the absence of the blocker.[1] Given these results, it seems unlikely that very high P_o of CRAC channels is causing a gross underestimation of the single channel current. Thus, from the results of noise analysis, we estimate that the monovalent conductance of the CRAC channel is ~0.2 pS.

DISCUSSION

In the absence of extracellular divalent cations, removal of intracellular Mg^{2+} during whole-cell recording activates a large monovalent current in T cells and RBL cells. This large Mg^{2+}-sensitive current has previously been attributed to monovalent permeation of CRAC channels, and its signature conductance and selectivity have been employed as a biophysical fingerprint to screen candidate CRAC channel genes. In this paper, we show that this large monovalent current, I_{MIC}, and the 40-pS channels that underlie it, differ in fundamental ways from I_{CRAC} and therefore represent a distinct ion channel type. These findings necessitate a re-

[1]The explanation for this is not clear, but it is not likely to be due to flickery block occurring at frequencies outside the recording bandwidth, since the fastest unbinding rate for a K_d of ~1 μM would be ~1,000 s^{-1} (assuming a maximum diffusion-limited on rate of 10^9 $M^{-1}s^{-1}$).

vision of the biophysical fingerprint of CRAC channels, and have important implications for studies of CRAC channel activation, permeation, and cellular function.

MIC and CRAC Currents Arise from Distinct Channels

A number of characteristics distinguish MIC channels from CRAC channels. These include the mode of activation, inhibition by Mg^{2+} or MgATP, kinetic properties, selectivity, pharmacology, and unitary conductance. These differences are summarized in Table I and are discussed below.

Several observations indicate that unlike I_{CRAC}, I_{MIC} is not store-operated (Figs. 2 and 3). For example, I_{MIC} slowly activates in cells in which I_{CRAC} is already preactivated by store depletion, and it activates even as I_{CRAC} deactivates due to store refilling. I_{MIC} is effectively suppressed by intracellular Mg^{2+} or MgATP, whereas CRAC channel gating is not noticeably affected. I_{MIC} activates about twice as slowly as I_{CRAC} in Jurkat cells; thus, the activation kinetics clearly do not reflect the time course of store depletion. Moreover, because introduction of 10 mM HEDTA into the cell would be expected to quickly buffer Mg^{2+}_i, it is unlikely that the time course of I_{MIC} is limited by the rate at which Mg^{2+} or MgATP are removed from the cell. Activation of single 40-pS channels after patch excision from RBL cells into a Mg^{2+}- and ATP-free solution can also be slow (Braun et al., 2001), suggesting that the rate-limiting step lies downstream of Mg^{2+} or MgATP removal. Interestingly, Mg^{2+} inhibits MIC channels more effectively in excised patches than in whole-cell recordings (Fig. 6), suggesting that the inhibition mechanism is more complex than simple channel blockade and may involve a diffusible molecule that is lost after patch excision.

Following removal of extracellular divalents, Na^+-I_{CRAC} is transient (Fig. 10 A), whereas I_{MIC} is relatively sustained (Fig. 5 C). The peak phase of the Na^+ current is linked to CRAC channels, based on its close correlation with Ca^{2+}-I_{CRAC} during store depletion and refilling (Fig. 8), and its sensitivity to SKF 96365 and 2-APB (Fig. 9). Na^+-I_{CRAC} depotentiated in DVF solutions to an average level of ~20%. We believe the steady-state activity is also from CRAC channels because its amplitude varies in parallel with the peak Na^+-I_{CRAC} and it has the same reversal potential, relative Cs^+ permeability and sensitivity to SKF 96365 and 2-APB, as the peak current. Although I_{MIC} is generally sustained under Mg^{2+}_i-free conditions after application of DVF solutions, it declines slowly in the presence of low levels of Mg^{2+}_i (0.5–1 mM; unpublished data). Thus, current decline under DVF conditions cannot be used as a specific indicator for I_{CRAC}.

Finally, the pharmacological signatures of I_{CRAC} and I_{MIC} also differ significantly (Figs. 4 and 9). SKF 96365 at micromolar levels is an effective blocker of I_{CRAC} (Franzius et al., 1994; Christian et al., 1996a), but not of I_{MIC}. High concentrations of 2-APB (20–40 μM) inhibit I_{CRAC} completely and irreversibly (Prakriya and Lewis, 2001), whereas they cause modest and rapidly reversible inhibition of I_{MIC}. Low concentrations of 2-APB (≤5 μM) which strongly enhance I_{CRAC} (Prakriya and Lewis, 2001) fail to affect I_{MIC}.

TABLE I

Characteristics of Distinguishing CRAC and MIC Channels

Property	CRAC channels	MIC channels
Store-dependent activation	yes	no
Inhibition by Mg^{2+}_i or MgATP	no	yes
Duration in DVF conditions	transient	sustained (with 0 Mg^{2+}_i)
Selectivity (P_{Cs}/P_{Na})	0.13	1.2
Inhibition by SKF 96365 (20 μM for 120 s)	87 ± 4%	10 ± 2%
Inhibition by 2-APB (IC_{50})	~10 μM, irreversible[a]	~50 μM, quickly reversible
Enhancement by 2-APB (EC_{50})	~3 μM[a]	none
Unitary current (Na^+, −110 mV)	−31 ± 2 fA (n = 10)	−4.5 ± 0.4 pA (n = 4)
Unitary chord conductance	~0.2 pS	44 ± 3 pS

[a]Results from Prakriya and Lewis (2001).

The rather large number of properties that distinguish the two conductances strongly suggest that I_{CRAC} and I_{MIC} arise from two different channels. However, an alternative explanation might be that removal of intracellular Mg^{2+} merely alters the properties of CRAC channels, making them acquire the characteristics of what we now call MIC channels (Kerschbaum and Cahalan, 1998). We do not believe that the MIC channel is an altered state of the CRAC channel for several key reasons. First, it seems unlikely that removal of Mg^{2+} alone would be able to alter such a diverse set of properties, including store-dependence, depotentiation, ion selectivity, pharmacological profile, and unitary conductance. Second, we find that removal of intracellular Mg^{2+} does not in fact reduce the selectivity of CRAC for Na^+ over Cs^+ (Fig. 10 C), nor does it prevent depotentiation of CRAC channels (i.e., make CRAC activity sustained) under 0-Ca^{2+}_o conditions (Figs. 2 A, 3 A, and 11 D). Finally, MIC channel activity is normal in mutant Jurkat cells that have very low levels of I_{CRAC}. Thus, the most parsimonious explanation for these data is that MIC and CRAC channels are separate and distinct proteins.[2]

In light of our results, various conclusions made in previous reports regarding the regulation of CRAC

[2]While this manuscript was under review, Hermosura et al. (2002) published evidence showing that the large sustained monovalent current in RBL cells perfused with Mg^{2+}-free intracellular solutions (termed MagNuM) can be separated from I_{CRAC}. This report and another (Bakowski and Parekh, 2002) also showed that intracellular Mg^{2+} does not significantly affect CRAC channel permeation in RBL cells, in agreement with our results.

channels probably apply more to MIC channels than to CRAC channels. For example, the voltage-dependent block of monovalent CRAC currents by extracellular Ca^{2+} (Kerschbaum and Cahalan, 1998; Fomina et al., 2000), the upregulation of CRAC channels in activated T cells (Fomina et al., 2000), and regulation by cytoplasmic Mg^{2+} and Ca^{2+} (Braun et al., 2001) were all measured under conditions optimized for activation of I_{MIC}. These issues may have to be revisited using recording conditions explicitly optimized for isolating the monovalent CRAC current. No specific inhibitors of I_{MIC} are yet known, but high intracellular Mg^{2+} (8–10 mM) or MgATP (>4 mM) effectively blocks I_{MIC} without affecting I_{CRAC}. It is important to note that moderate levels of Mg^{2+} (2–3 mM) commonly used in studies of I_{CRAC} may not be sufficient to completely eliminate MIC activity, as we often found 3–5 active MIC channels in Jurkat cells under these conditions. Although this represents a small fraction of the total MIC conductance in the cell, the unitary current of MIC channels is so much larger than that of CRAC channels that it can seriously contaminate noise measurements under DVF conditions (see below). Activity of MIC channels can also lead to inadvertent contamination of I_{CRAC} in the presence of divalent ions, although appropriate subtraction of the "leak" current can alleviate this problem (see MATERIALS AND METHODS).

I_{MIC} May Arise from TRP-PLIK/LTRPC7 Channels

Given that MIC channels are distinct from CRAC, what is their molecular identity? Recently, a novel member of the TRP family of ion channels has been cloned which has been named TRP-PLIK (Runnels et al., 2001) or LTRPC7 (Nadler et al., 2001). Several characteristics of TRP-PLIK/LTRPC7 are similar to MIC in Jurkat cells. LTRPC7 is expressed in cell lines commonly employed for studies of I_{CRAC}, such as Jurkat T cells and RBL cells. Activation of LTRPC7 in transfected cells is elicited by whole-cell dialysis with chelators of Mg^{2+}, and introduction of Mg^{2+} and/or Mg-ATP inhibits its channel activity (Nadler et al., 2001). TRP-PLIK/LTRPC7 produces a nonselective cation channel with strong outward rectification in the presence of extracellular divalent ions (Nadler et al., 2001; Runnels et al., 2001), much like the outward rectification of I_{MIC} we observe under similar conditions (Fig. 7). Elimination of extracellular Ca^{2+} or Na^+ alone does not affect the inward current through LTRPC7 (Nadler et al., 2001) or MIC channels (Fig. 7 C and unpublished data). Together, these similarities to I_{MIC} in Jurkat cells suggest that TRP-PLIK/LTRPC7 encodes the MIC channel.

The activation mechanism and physiological roles of MIC channels are not well understood at this point. A small number of MIC channels appear to be active in resting Jurkat cells, based on the current seen in DVF conditions immediately after break-in with 0-Mg^{2+} pipette solution (Fig. 6 A). Although depletion of cytoplasmic Mg^{2+} can further activate MIC channels, it seems unlikely that this is the physiological stimulus (see Nadler et al., 2001), as cytosolic Mg^{2+} in many cells is held relatively constant between 0.5 and 1 mM (Romani and Scarpa, 2000). Its sensitivity to inhibition by Mg^{2+}-nucleotides has led to the hypothesis that it opens in response to declining ATP levels (Nadler et al., 2001), but there is also evidence that channel activation requires kinase activity of the COOH-terminal PLIK domain (Runnels et al., 2001). The physiological consequences of MIC activation are also unclear. Nadler et al. (2001) have proposed that LTRPC7 provides a conduit for Ca^{2+} entry that regulates mitochondrial activity and ATP homeostasis (Nadler et al., 2001). However, the precise Ca^{2+} permeability of this channel has not been measured. Although it has been stated that the block of Na^+ flux by external divalent ions renders LTRPC7 solely permeable to divalent ions at negative potentials (Nadler et al., 2001), our preliminary experiments on MIC channels in Jurkat cells suggest that Na^+ can carry inward current in the presence of $Mg^{2+}{}_o$ (unpublished data). Thus, while MIC channels may provide a pathway for Ca^{2+} entry, they may also depolarize the cell by conducting monovalent ions. From the relative amplitudes of the single-channel and whole-cell currents we estimate that Jurkat cells express ~250–500 MIC channels per cell.

Intracellular Mg^{2+} and CRAC Channel Function

In previous studies, the removal of intracellular Mg^{2+} under DVF conditions appeared to change a small transient and Na^+-selective current through CRAC channels into a much larger, sustained, and nonselective current with equal permeability to Cs^+ and Na^+ (Lepple-Wienhues and Cahalan, 1996; Kerschbaum and Cahalan, 1998). These observations were interpreted to mean that $Mg^{2+}{}_i$ removal prevents depotentiation of CRAC and alters their selectivity. We have found that intracellular Mg^{2+} does not affect Ca^{2+}-dependent potentiation of CRAC channels, or the reverse process of depotentiation (Fig. 11), nor is it required to achieve selectivity for Na^+ over Cs^+ (Fig. 10 C). This discrepancy with the earlier results can now be explained by the fact that removal of $Mg^{2+}{}_i$ activates I_{MIC}, which is much larger, more sustained, and less selective than I_{CRAC}.

The Unitary Conductance of CRAC Channels

Our results indicate that the monovalent conductance of CRAC channels is too small to be resolvable in whole-cell recordings. Noise analysis of whole-cell Na^+-I_{CRAC} suggests a conductance in the range of ~0.2 pS. This is dramatically different from recent reports in T cells and RBL cells, where a conductance of ~40 pS was

reported for monovalent currents through CRAC channels (Kerschbaum and Cahalan, 1999; Fomina et al., 2000; Braun et al., 2001). This discrepancy is explained by the fact that the earlier experiments were performed in the absence of cytoplasmic Mg^{2+}, which as we have shown here activates store-independent MIC channels. Our estimate of the unitary conductance is also smaller than an earlier estimate of 2.6 pS based on noise analysis (Lepple-Wienhues and Cahalan, 1996). Using the ionic conditions of this earlier study (3 mM intracellular Mg^{2+} + 1 μM extracellular Mg^{2+}), we also detect a significantly larger noise, which appears to arise from flickery block of several active MIC channels in the cell. Thus, even slight contamination of Na^+-I_{CRAC} with I_{MIC} may lead to large differences in the estimated unitary currents.

We considered several possible factors that could lead us to underestimate the unitary currents. Current fluctuations could be missed if they occur at frequencies outside the recording bandwidth. However, spectral analysis showed that most of the power of the current noise occurred at frequencies <1 kHz, well within the recording bandwidth (Fig. 12 E). A more difficult problem could arise if activation of I_{CRAC} occurs through an increase in N, the number of activatable channels, each of which has a high open probability and therefore contributes little noise. However, we were unable to detect discrete jumps in current during the activation or depotentiation of monovalent I_{CRAC}. In addition, partial inhibition of monovalent I_{CRAC} with 1 μM extracellular Ca^{2+} did not increase the noise, indicating that whatever the mechanism of activation, the P_o of active CRAC channels conducting Na^+ is quite small. Together with our estimates of the single channel conductance, these observations set limits on the maximum size of the single-channel conductance to <1 pS.

Our estimate of −3.8 fA at −110 mV for the unitary Ca^{2+} current compares well with a previous estimate in 110 mM $Ca^{2+}{}_o$ at −80 mV (−3.7 fA) (Zweifach and Lewis, 1993). Note that this estimate is roughly eightfold smaller than the single-channel estimates of the Na^+ current given above (−31 fA). The fact that the whole-cell Na^+-I_{CRAC} is also about eightfold larger than Ca^{2+}-I_{CRAC} suggests that the increase in whole-cell current seen upon exchanging the $Ca^{2+}{}_o$ solution for the DVF solution can entirely be accounted for by the increase in conductance of the CRAC channels without a significant change in channel P_o. From the ratio of the unitary and whole-cell peak Na^+ currents, we estimate that the number of CRAC channels per cell is at least 5,000–10,000. More would be expected if the open probability is low, as is suggested by the linear relation of variance to mean current. Finally, it should be noted that our estimate for the unitary conductance of Na^+-I_{CRAC} (0.2 pS) is significantly smaller than the 42-pS conductance reported for the CaT1 channel under similar DVF conditions (Yue et al., 2001), consistent with recent suggestions that CaT1 may not comprise the complete CRAC-channel pore (Voets et al., 2001).

Selectivity of CRAC Channels

Similarities and differences between the permeation properties of CRAC channels and voltage-gated Ca^{2+} (Ca_V) channels have interesting implications for mechanisms of ion selectivity in CRAC channels. Under physiological conditions, Ca_V channels have an extremely high selectivity for Ca^{2+} over monovalent ions ($P_{Ca}/P_{Na} > 1{,}000$). The high Ca^{2+} selectivity is thought to arise from the high-affinity binding of Ca^{2+} within the pore, which prevents Na^+ from conducting. In fact, the removal of extracellular divalent ions allows Na^+ to conduct freely (Almers and McCleskey, 1984; Hess and Tsien, 1984). CRAC channels show a comparably high selectivity for Ca^{2+} over monovalent ions (Hoth and Penner, 1993), and similarly become freely permeable to Na^+ in the absence of extracellular divalents. Thus, it is likely that the Ca^{2+} selectivity of CRAC channels also arises from high affinity Ca^{2+} binding within the pore, and this is consistent with the ability of 1 μM Ca^{2+} to block Na^+-I_{CRAC} by ∼50% (see RESULTS).

The most obvious differences between the two channels relates to their unitary conductances and permeability to Cs^+. Ca_V channels have single-channel conductances for Ca^{2+} in the range of 5–20 pS and ∼85 pS for Na^+ under DVF conditions (Hess et al., 1986). By contrast, the unitary conductances of CRAC channels is estimated to be ∼21 fS for Ca^{2+} and 0.2 pS for Na^+, or ∼500-fold smaller than Ca_V channels. In addition, under DVF conditions Ca_V channels readily pass Cs^+ (P_{Cs}/P_{Na} ∼0.6; Hess et al., 1986), whereas CRAC channels do not ($P_{Cs}/P_{Na} = 0.13$; Fig. 10; see also Lepple-Wienhues and Cahalan, 1996). These observations suggest that although CRAC channels and voltage-gated Ca^{2+} channels achieve selectivity for Ca^{2+} over other ions by high affinity Ca^{2+} binding within the pore, many structural features may be significantly different between these two channel types.

What unique structural features of CRAC channels could give rise to such a low conductance? A popular model proposes that the high throughput of Ca_V channels arises from ion–ion interactions as ions move single-file through the pore (Tsien et al., 1987). Thus, one possibility is that weak ion–ion interactions underlie the low flux rate of Ca^{2+} through CRAC channels. However, this idea cannot adequately explain why CRAC channels would have an equally low conductance for monovalent ions. We hypothesize that CRAC channels possess a nonselective rate-limiting barrier to ion permeation in series with the selectivity filter. Such a barrier may explain not only the uniformly low per-

meability to various ions, but also the lack of permeability to Cs^+. Identification of CRAC channel genes will provide much needed tools for elucidating the mechanism of CRAC channel permeation. In the interim, systematic examination of permeation of various ions through native CRAC channels will improve our understanding of the properties of the channel pore.

The authors would like to thank K. Mikoshiba for the gift of 2-APB. We thank members of the Lewis lab for helpful discussions and Dr. Rick Aldrich, Dr. Adam Zweifach, and Diana Bautista for comments on the manuscript.

This work was supported by a postdoctoral fellowship from the Irvington Foundation for Immunological Research to M. Prakriya and National Institutes of Health grant GM45374 to R.S. Lewis.

Submitted: 27 December 2001
Revised: 1 April 2002
Accepted: 3 April 2002

REFERENCES

Almers, W., and E.W. McCleskey. 1984. Non-selective conductance in calcium channels of frog muscle: calcium selectivity in a single-file pore. *J. Physiol.* 353:585–608.

Bakowski, D., and A.B. Parekh. 2002. Monovalent cation permeability and Ca^{2+} block of the store-operated Ca^{2+} current I_{CRAC} in rat basophilic leukemia cells. *Pflügers Arch.* 443:892–902.

Braun, F.J., L.M. Broad, D.L. Armstrong, and J.W. Putney, Jr. 2001. Stable activation of single Ca^{2+} release-activated Ca^{2+} channels in divalent cation-free solutions. *J. Biol. Chem.* 276:1063–1070.

Broad, L.M., F.J. Braun, J.P. Lievremont, G.S. Bird, T. Kurosaki, and J.W. Putney, Jr. 2001. Role of the phospholipase C-inositol 1,4,5-trisphosphate pathway in calcium release-activated calcium current and capacitative calcium entry. *J. Biol. Chem.* 276:15945–15952.

Christian, E.P., K.T. Spence, J.A. Togo, P.G. Dargis, and E. Warawa. 1996a. Extracellular site for econazole-mediated block of Ca^{2+} release-activated Ca^{2+} current (I_{crac}) in T lymphocytes. *Br. J. Pharmacol.* 119:647–654.

Christian, E.P., K.T. Spence, J.A. Togo, P.G. Dargis, and J. Patel. 1996b. Calcium-dependent enhancement of depletion-activated calcium current in Jurkat T lymphocytes. *J. Membr. Biol.* 150:63–71.

Clapham, D.E., L.W. Runnels, and C. Strubing. 2001. The trp ion channel family. *Nat. Rev. Neurosci.* 2:387–396.

Fanger, C.M., M. Hoth, G.R. Crabtree, and R.S. Lewis. 1995. Characterization of T cell mutants with defects in capacitative calcium entry: genetic evidence for the physiological roles of CRAC channels. *J. Cell Biol.* 131:655–667.

Feske, S., J. Giltnane, R. Dolmetsch, L.M. Staudt, and A. Rao. 2001. Gene regulation mediated by calcium signals in T lymphocytes. *Nat. Immunol.* 2:316–324.

Fomina, A.F., C.M. Fanger, J.A. Kozak, and M.D. Cahalan. 2000. Single channel properties and regulated expression of Ca^{2+} release-activated Ca^{2+} (CRAC) channels in human T cells. *J. Cell Biol.* 150:1435–1444.

Franzius, D., M. Hoth, and R. Penner. 1994. Non-specific effects of calcium entry antagonists in mast cells. *Pflügers Arch.* 428:433–438.

Hermosura, M.C., M.K. Monteilh-Zoller, A.M. Scharenberg, R. Penner, and A. Fleig. 2002. Dissociation of the store-operated calcium current I_{CRAC} and the Mg^{2+}-nucleotide-regulated metal ion current MagNuM. *J. Physiol.* 539:445–458.

Hess, P., and R.W. Tsien. 1984. Mechanism of ion permeation through calcium channels. *Nature.* 309:453–456.

Hess, P., J.B. Lansman, and R.W. Tsien. 1986. Calcium channel selectivity for divalent and monovalent cations. Voltage and concentration dependence of single channel current in ventricular heart cells. *J. Gen. Physiol.* 88:293–319.

Hoth, M. 1995. Calcium and barium permeation through calcium release-activated calcium (CRAC) channels. *Pflügers Arch.* 430: 315–322.

Hoth, M., and R. Penner. 1993. Calcium release-activated calcium current in rat mast cells. *J. Physiol.* 465:359–386.

Jackson, P.S., and K. Strange. 1995. Single-channel properties of a volume-sensitive anion conductance. Current activation occurs by abrupt switching of closed channels to an open state. *J. Gen. Physiol.* 105:643–660.

Kerschbaum, H.H., and M.D. Cahalan. 1998. Monovalent permeability, rectification, and ionic block of store-operated calcium channels in Jurkat T lymphocytes. *J. Gen. Physiol.* 111:521–537.

Kerschbaum, H.H., and M.D. Cahalan. 1999. Single-channel recording of a store-operated Ca^{2+} channel in Jurkat T lymphocytes. *Science.* 283:836–839.

Lepple-Wienhues, A., and M.D. Cahalan. 1996. Conductance and permeation of monovalent cations through depletion-activated Ca^{2+} channels (I_{CRAC}) in Jurkat T cells. *Biophys. J.* 71:787–794.

Lewis, R.S. 1999. Store-operated calcium channels. *Adv. Second Messenger Phosphoprotein Res.* 33:279–307.

Lewis, R.S. 2001. Calcium signaling mechanisms in T lymphocytes. *Annu. Rev. Immunol.* 19:497–521.

Ma, H.T., R.L. Patterson, D.B. van Rossum, L. Birnbaumer, K. Mikoshiba, and D.L. Gill. 2000. Requirement of the inositol trisphosphate receptor for activation of store-operated Ca^{2+} channels. *Science.* 287:1647–1651.

Nadler, M.J., M.C. Hermosura, K. Inabe, A.L. Perraud, Q. Zhu, A.J. Stokes, T. Kurosaki, J.P. Kinet, R. Penner, A.M. Scharenberg, and A. Fleig. 2001. LTRPC7 is a Mg.ATP-regulated divalent cation channel required for cell viability. *Nature.* 411:590–595.

Parekh, A.B., and R. Penner. 1997. Store depletion and calcium influx. *Physiol. Rev.* 77:901–930.

Partiseti, M., F. Le Deist, C. Hivroz, A. Fischer, H. Korn, and D. Choquet. 1994. The calcium current activated by T cell receptor and store depletion in human lymphocytes is absent in a primary immunodeficiency. *J. Biol. Chem.* 269:32327–32335.

Prakriya, M., and R.S. Lewis. 2001. Potentiation and inhibition of Ca^{2+} release-activated Ca^{2+} channels by 2-aminoethyldiphenyl borate (2-APB) occurs independently of IP_3 receptors. *J. Physiol.* 536:3–19.

Prakriya, M., and R.S. Lewis. 2002. Store-operated calcium channels: properties, functions and the search for a molecular mechanism. *In* Molecular Insights into Ion Channel Biology in Health and Disease. R. Maue, editor. Elsevier Science, Amsterdam. In press.

Putney, J.W., Jr., and R.R. McKay. 1999. Capacitative calcium entry channels. *Bioessays.* 21:38–46.

Putney, J.W., Jr., L.M. Broad, F.J. Braun, J.P. Lievremont, and G.S. Bird. 2001. Mechanisms of capacitative calcium entry. *J. Cell Sci.* 114:2223–2229.

Romani, A.M., and A. Scarpa. 2000. Regulation of cellular magnesium. *Front. Biosci.* 5:D720–D734.

Runnels, L.W., L. Yue, and D.E. Clapham. 2001. TRP-PLIK, a bifunctional protein with kinase and ion channel activities. *Science.* 291:1043–1047.

Rychkov, G., H.M. Brereton, M.L. Harland, and G.J. Barritt. 2001. Plasma membrane Ca^{2+} release-activated Ca^{2+} channels with a high selectivity for Ca^{2+} identified by patch-clamp recording in rat liver cells. *Hepatology.* 33:938–947.

Sigworth, F.J. 1980. The variance of sodium current fluctuations at the node of Ranvier. *J. Physiol.* 307:97–129.

Tsien, R.W., P. Hess, E.W. McCleskey, and R.L. Rosenberg. 1987. Calcium channels: mechanisms of selectivity, permeation, and

block. *Annu. Rev. Biophys. Biophys. Chem.* 16:265–290.

Voets, T., J.Prenen, A. Fleig, R. Vennekens, H. Watanabe, J.G. Hoenderop, R.J. Bindels, G. Droogmans, R. Penner, and B. Nilius. 2001. CaT1 and the calcium release-activated calcium channel manifest distinct pore properties. *J. Biol. Chem.* 276:47767–47770.

Yue, L., J.B. Peng, M.A. Hediger, and D.E. Clapham. 2001. CaT1 manifests the pore properties of the calcium-release-activated calcium channel. *Nature.* 410:705–709.

Zweifach, A., and R.S. Lewis. 1993. Mitogen-regulated Ca^{2+} current of T lymphocytes is activated by depletion of intracellular Ca^{2+} stores. *Proc. Natl. Acad. Sci. USA.* 90:6295–6299.

Zweifach, A., and R.S. Lewis. 1995. Slow calcium-dependent inactivation of depletion-activated calcium current. Store-dependent and -independent mechanisms. *J. Biol. Chem.* 270:14445–14451.

Zweifach, A., and R.S. Lewis. 1996. Calcium-dependent potentiation of store-operated calcium channels in T lymphocytes. *J. Gen. Physiol.* 107:597–610.